Petrography, geochemistry and geochronology of igneous rocks from the Jiangnan Orogen, South China: constraints on the Early Paleozoic tectonic evolution of the South China Block

Yuanyuan Tang[1,2], Yu Shi[1,2]*, Boyin Weng[1,2], Yuxi Zhou[1,2] and Yuanchun Lan[1,2]

[1]Guangxi Key Laboratory of Hidden Metal Mineral Exploration, Guilin University of Technology, Guilin, China, [2]Collaborative Innovation Center for Exploration of Nonferrous Metal Deposits and Efficient Utilization of Resources, Guilin University of Technology, Guilin, China

The Early Paleozoic tectonic evolution of the South China Block (SCB) remains controversial related to intracontinental orogenic and oceanic subduction processes. We present whole-rock major and trace elemental data, LA-ICP-MS zircon U-Pb age and Lu-Hf isotopic data for the Early Paleozoic igneous rocks including granodiorites from the Yuechengling pluton and volcanic breccias from the Damingshan pluton from the western segment of the Jiangnan Orogen in the SCB. LA-ICP-MS zircon U-Pb dating yielded emplacement ages for the Yuechengling S-type granitoids of 438−436 Ma and the deposited age for the Damingshan volcaniclastic rocks to be later than 451 Ma. The Yuechengling granitoids have consistent SiO_2, TiO_2, $Fe_2O_3^T$, MgO, and P_2O_5 contents, higher Al_2O_3 contents, and $Na_2O + K_2O$ values, but lower $Mg^{\#}$ values, compared with those of the Damingshan volcaniclastic rocks. All the studied samples exhibit enrichment in LREEs and moderate negative Eu anomalies ($\delta Eu = 0.63−0.75$), with negative Ba, Sr, Nb, Ta, P, and Ti anomalies, and positive Rb, Th, U, Pb, and K anomalies. The granitoids have variable CaO/Na_2O ratios of 0.22−1.11, negative $\varepsilon_{Hf}(t)$ values of −11.98 to −0.90, and corresponding T_{DM2} ages distributed from 2.37 to 1.55 Ga. The petrographic and geochemical characteristics of the Yuechengling granitoids indicate that their parental magma was derived from a crustal meta-greywacke and meta-pelite components in the Paleoproterozoic basement, and have undergone some degree of fractional crystallization. The volcaniclastic rocks have mostly negative $\varepsilon_{Hf}(t)$ values with partially positive (−27.54 to 8.73), and zircons with negative $\varepsilon_{Hf}(t)$ values (−27.54 to −0.14) show T_{DM2} ages of 3.79 to 1.63 Ga. Combined with petrographic and geochemical data, we suggest that the Damingshan volcaniclastic rocks were derived from Neoarchean-Neoproterozoic crustal materials and the felsic parental magma has undergone some degree of magma mixing with mantle material, and deposited soon after a Late Ordovician volcanic eruption (later than 451 Ma). Integrated with previous studies, our new data support the intracontinental orogenic model to account for the Early Paleozoic tectonic evolution. Thus, we suggest that the Early Paleozoic tectonic setting of the SCB was intracontinental orogeny rather than oceanic subduction-collision.
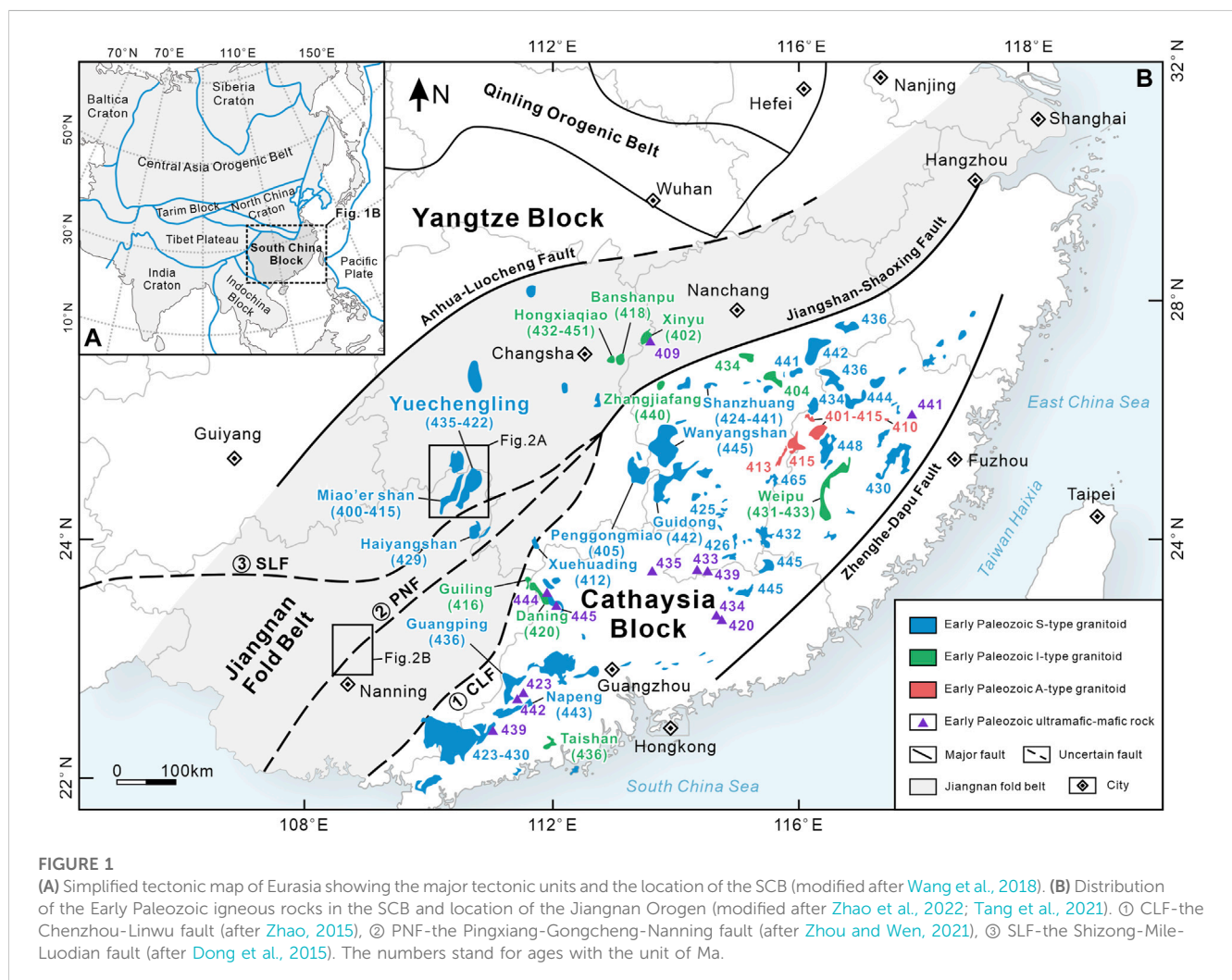
1 Introduction

The SCB, a major continental block of East Asia, is located in southeast Eurasia and the convergence area of Eurasian and Pacific Plates (Figure 1A). The block consists of the Yangtze Block to the northwest and the Cathaysia Block to the southeast, which were welded together during the Neoproterozoic along the Jiangnan fold belt (the Jiangnan Orogen, Figure 1B) (Charvet, 2013; Yao et al., 2014; Shu et al., 2015). The SCB had undergone three episodes of tectonic evolution of the Proto-(Early Paleozoic), the Paleo-(Late Paleozoic) and the Neo-(Mesozoic-Cenozoic) Tethys since Neoproterozoic, corresponding to three tectonic evolution stages of the Caledonian (Early Paleozoic), Indosinian (Early Mesozoic) and Yanshanian-Himalayan (Late Mesozoic-Cenozoic) (Zhang et al., 2013). As the first extensive tectono-thermal event in the SCB since the Neoproterozoic break-up of the Rodinia supercontinent (Wang et al., 2011; Huang et al., 2013; Yu et al., 2016), the Early Paleozoic orogeny strongly affected the final tectonic framework of the SCB (Shu, 2012; Zhang et al., 2013),

which is characterized by high-grade metamorphism, intensive deformation, wide-spread magmatism and unconformities (Charvet et al., 2010; Liu et al., 2010; Wang et al., 2011; Zhang et al., 2015; Tang et al., 2021).

Despite decades of considerable research, the Early Paleozoic orogeny remains uncertain with regard to its tectonic setting and geodynamic driving force (Charvet et al., 2010; Wang et al., 2010; Huang et al., 2013; Shu et al., 2014; Yu et al., 2016). Two opposing tectonic setting models of oceanic subduction-collision and intracontinental orogeny are proposed, controversy still exists regarding the Early Paleozoic "Huanan Ocean" in the SCB. Some researchers proposed that the Yangtze and Cathaysia Blocks were amalgamated together into the ancient South China continent during the amalgamation process of the Rodinia supercontinent in the Late Neoproterozoic and the Early Paleozoic "Huanan Ocean" did not exist (e.g., Charvet et al., 2010; Huang et al., 2013; Xia et al., 2014; Shu et al., 2015; Tang et al., 2021). While others believed that the "Huanan Ocean" existed in the Early Paleozoic and the oceanic subduction occurred (e.g., Hsü et al., 1990; Qin et al., 2011; Peng

FIGURE 1
(A) Simplified tectonic map of Eurasia showing the major tectonic units and the location of the SCB (modified after Wang et al., 2018). **(B)** Distribution of the Early Paleozoic igneous rocks in the SCB and location of the Jiangnan Orogen (modified after Zhao et al., 2022; Tang et al., 2021). ① CLF-the Chenzhou-Linwu fault (after Zhao, 2015), ② PNF-the Pingxiang-Gongcheng-Nanning fault (after Zhou and Wen, 2021), ③ SLF-the Shizong-Mile-Luodian fault (after Dong et al., 2015). The numbers stand for ages with the unit of Ma.

et al., 2016a; Peng et al., 2016b; Liu et al., 2018). Based on the Early Paleozoic ultramafic-mafic rocks (e.g., Yao et al., 2012; Wang et al., 2013b; Zhang et al., 2015) and I-type granitoids (e.g., Huang et al., 2013; Zhang et al., 2015; Yu et al., 2016; Tang et al., 2021), a model of the Early Paleozoic magmatic activity in the SCB was related to the partially molten SCLM (Sub-Continental Lithospheric Mantle) heated by upwelling asthenosphere triggered by lithospheric delamination is proposed. However, there was no consensus concerning the geodynamic framework of the Early Paleozoic orogeny.

The Jiangnan Orogen is located in the southeastern margin of the Yangtze Block and is bound on its southeastern side by the Cathaysia Block along the Jiangshan-Shaoxing fault as the eastern boundary, with a width of ca. 120 km and length of ca. 1,500 km (Figure 1B; Wang X. L. et al., 2007; Yao et al., 2014), which could be divided into the eastern and western segments by the border of Hunan and Jiangxi provinces. Due to poor exposure and thermo-tectonic modification (Li et al., 2010; Shu, 2012), the southwestern boundary of the western segment is unclear and several faults have been proposed, such as the Pingxiang-Gongcheng-Nanning fault (e.g., Zhou and Wen, 2021), the Chenzhou-Linwu fault (e.g., Zhao, 2015), and the Shizong-Mile-Luodian fault (e.g., Dong et al., 2015). The Jiangnan Orogen is considered to represent the subductional-collisional suture between the Yangtze and Cathaysia Blocks (Yao et al., 2014), which is a key to understanding the assembly and evolution of the SCB (Wang X. L. et al., 2007; Lin et al., 2008; Charvet et al., 2010; Zhao et al., 2016). Therefore, the temporal-spatial pattern and petrogenesis of the Early Paleozoic igneous rocks in the western segment can provide particular constraints on the tectonic setting and evolution of the Early Paleozoic orogeny (Wang et al., 2010; Wang et al., 2013a; Zhong et al., 2013; Shu et al., 2014; Shu et al., 2015). Moreover, previous studies are mostly focused on the granitoids in the SCB (e.g., Huang et al., 2013; Zhao et al., 2013; Zhong et al., 2013; Yu et al., 2016; Cai et al., 2017; Xin et al., 2020; Tang et al., 2021), while less attention has been paid on the Early Paleozoic volcanic-volcaniclastic rocks. Consequently, we studied the Early Paleozoic intrusive and extrusive rocks located in northeastern and central Guangxi province in the western segment, which are of great significance for constraining the Early Paleozoic magmatism, tectonic evolution, and geodynamic driving force of the SCB. Based on field geological investigation, we present new zircon U-Pb ages, Hf isotopic compositions, and whole-rock geochemical data for the Early Paleozoic igneous rocks to reveal their petrogenesis, and further offer new perspectives on the Early Paleozoic tectonic setting of the SCB.

2 Geological setting and sample descriptions

The Yangtze and Cathaysia Blocks were amalgamated and separated in multiple tectonic evolutions from the Mesoproterozoic to Neoproterozoic (Charvet et al., 1996; Wang et al., 2011; Shu, 2012; Shu et al., 2014; Shu et al., 2015). The basement of the Yangtze Block is Archean tonalitic-trondhjemitic-granodioritic (TTG) gneisses with ages of 3.2–2.9 Ga in the north (e.g., the Kongling Group) and Paleoproterozoic strata in the west (e.g., the Hekou Group), overlain by a Neoproterozoic to Cenozoic
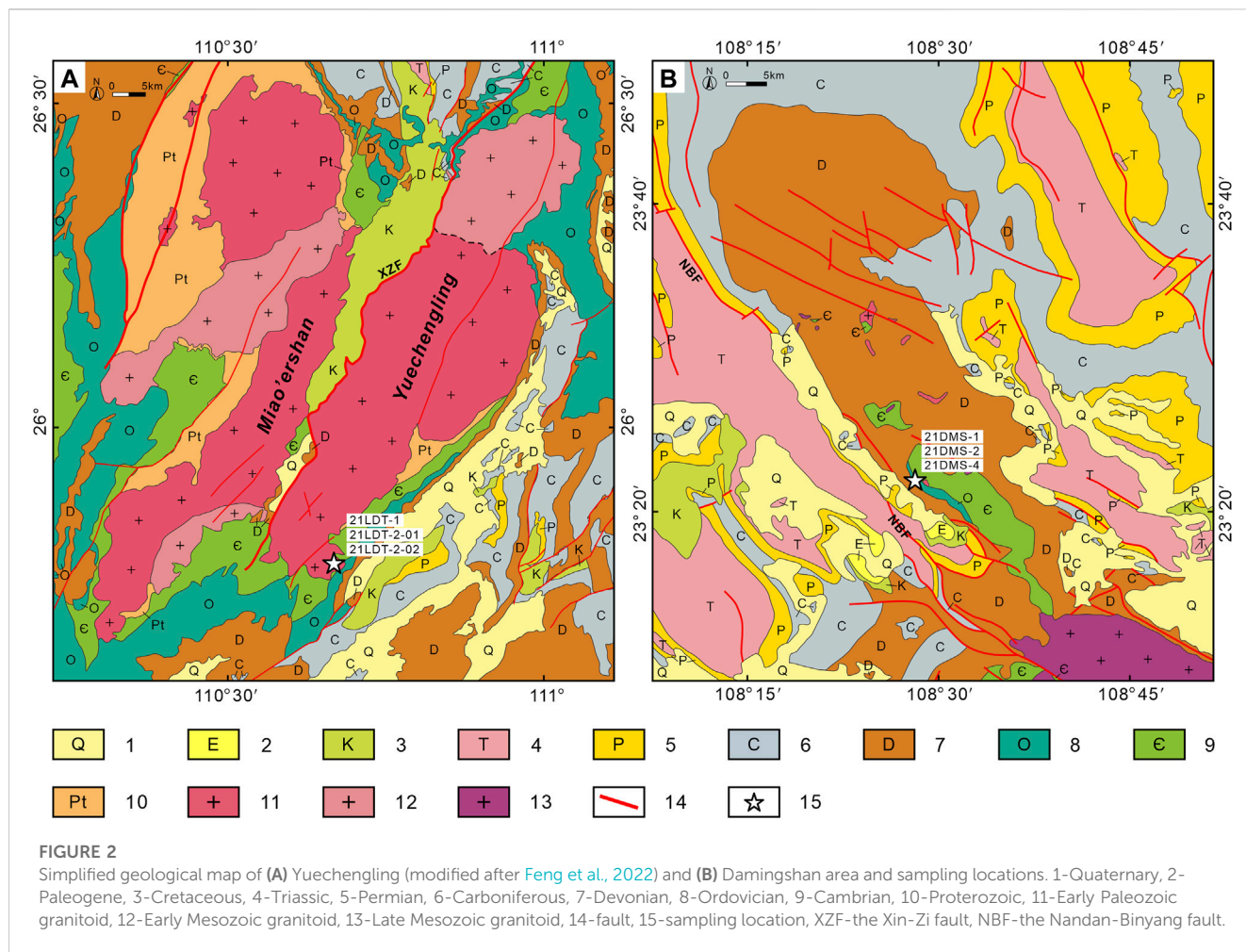
cover (Qiu et al., 2000; Jiao et al., 2009; Wang et al., 2013b; Tang et al., 2021). The basement of the Cathaysia Block has a Paleoproterozoic origin (1.8–2.0 Ga), which is dominantly composed of schist, gneiss, amphibolite, migmatite and volcaniclastics (Liu et al., 2009; Yu et al., 2009; Yu et al., 2010; Wang et al., 2013b), while the Jiangnan Orogen consists mostly of the Paleoproterozoic to Early Neoproterozoic sedimentary strata and igneous rocks (Wang et al., 2008; Shu et al., 2015; Zhao et al., 2022).

Most of the Early Paleozoic igneous rocks in the SCB are distributed in southeastern margin of the Yangtze Block (the Jiangnan Orogen) and northwestern-western margin of the Cathaysia Block (Figure 1B). Recently, the increasing discovery of S-type (e.g., Wang et al., 2011; Zhang et al., 2012; Shu et al., 2015), I-type (e.g., Huang et al., 2013; Zhong et al., 2013; Zhang et al., 2015; Yu et al., 2016; Tang et al., 2021), and A-type (Feng et al., 2014; Cai et al., 2017; Xin et al., 2020) granitoids, ultramafic-mafic (Wang et al., 2013b; Zhong et al., 2013; Zhong et al., 2014; Zhong et al., 2016; Zhang et al., 2015), and intermediate (Zhong et al., 2016) intrusive rocks, volcanic rocks (Yao et al., 2012; Zhang X. S. et al., 2017; Qin et al., 2017; Liu et al., 2018), and metamorphic rocks (Wang Y. J. et al., 2007; Li et al., 2011) from the SCB have been reported. Geochronological studies indicate that the magmatism in the Early Paleozoic initiated in the Late Ordovician (ca. 460 Ma) and lasted until the Late Devonian (ca. 390 Ma) (Li et al., 2011; Wang et al., 2013b; Xin et al., 2020; Kong et al., 2021; Tang et al., 2021 and the related references).

In this study, granitoids from the Yuechengling pluton and volcaniclastic rocks from the Damingshan pluton located in the western segment of the Jiangnan Orogen were studied (Figure 1B), aiming to constrain the petrogenesis of the igneous rocks and offer new perspectives on the tecno-thermal evolution and tectonic setting of the Early Paleozoic magmatic activity in the SCB. The sampling locations and mineral compositions of the samples are shown in Figure 2 and Table 1.

2.1 The Yuechengling pluton

The Yuechengling pluton is located in the border region of Guangxi and Hunan Provinces, which is mainly composed of the Early Paleozoic granitoids with a surface area of more than 3,000 km² (Wu et al., 2012; Chen et al., 2016). It showed a NEE-trending distribution with the outcropped strata of Proterozoic (Pt), Cambrian (Є), Ordovician (O), Devonian (D), Carboniferous (C), Permian (P), Cretaceous (K), and Quaternary (Q) (Figure 2A). There are two episodes of granitic magmatic activities and the Early Paleozoic (435–422 Ma) granite (Zhao et al., 2013; Bai et al., 2015; Chen et al., 2016 and the related references) in the south and associated Early Mesozoic (236–222 Ma) granite (Chu et al., 2012; Feng et al., 2022 and the related references) in the north were produced respectively. Many deposits of W-Sn-Mo-Pb-Zn-Cu are surrounding the contact zone between the pluton and strata, forming an ore-rich belt around the Yuechengling pluton (Wu et al., 2012; Chen et al., 2016). Many scholars have constrained the geochronological, lithological, geochemical, petrogenesis (e.g., Zhao et al., 2013; Bai et al., 2015; Chen et al., 2016) and mineralization of non-ferrous metals (e.g., Chen et al., 2016;
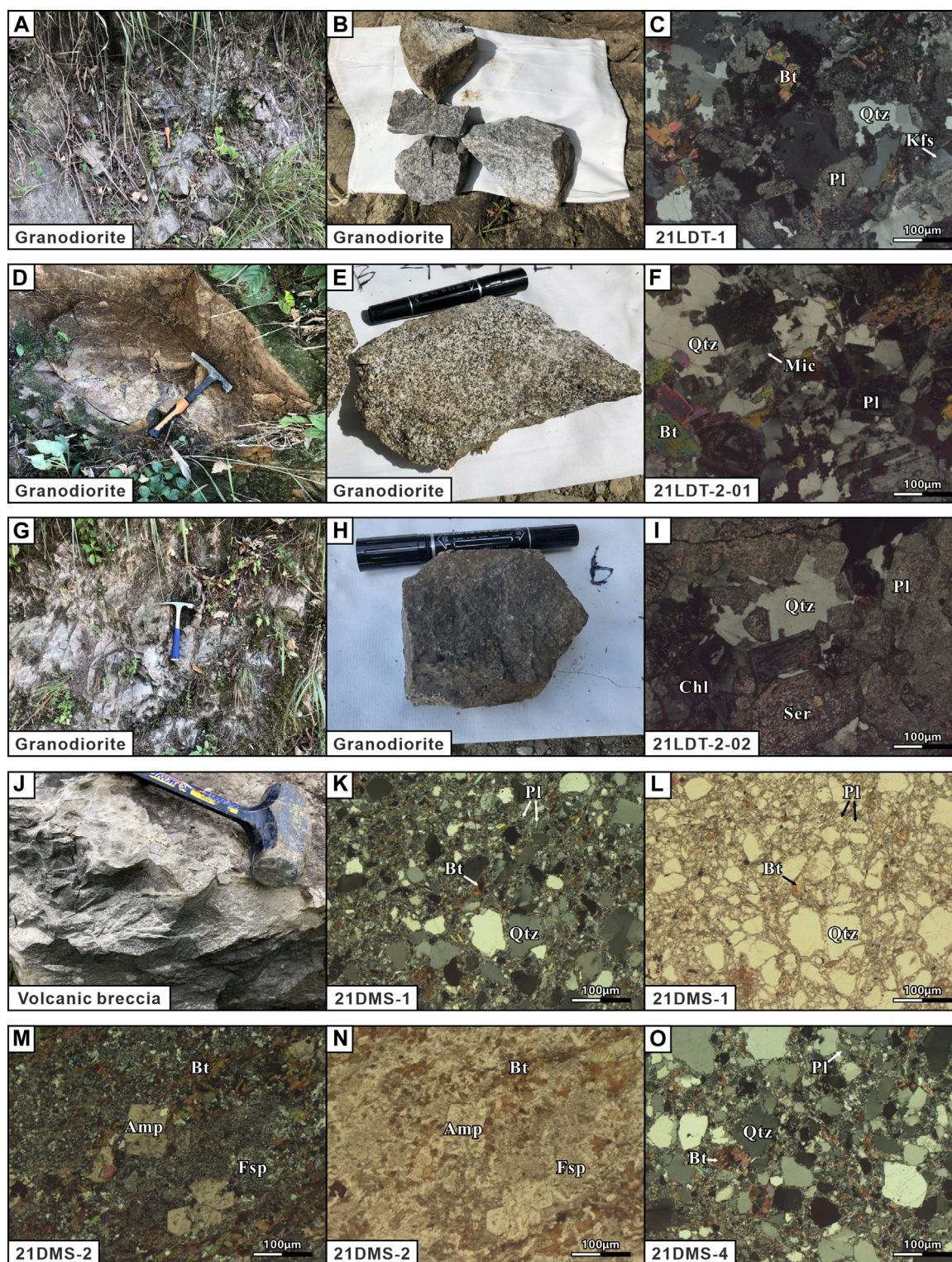
FIGURE 2
Simplified geological map of **(A)** Yuechengling (modified after Feng et al., 2022) and **(B)** Damingshan area and sampling locations. 1-Quaternary, 2-Paleogene, 3-Cretaceous, 4-Triassic, 5-Permian, 6-Carboniferous, 7-Devonian, 8-Ordovician, 9-Cambrian, 10-Proterozoic, 11-Early Paleozoic granitoid, 12-Early Mesozoic granitoid, 13-Late Mesozoic granitoid, 14-fault, 15-sampling location, XZF-the Xin-Zi fault, NBF-the Nandan-Binyang fault.

TABLE 1 The sampling location, lithology and mineral assemblages of the Yuechengling granitoids and the Damingshan volcaniclastic rocks.

Pluton	Sample NO.	Lithology	Location	Mineralogy
Yuechengling	21LDT-1	granodiorite	N25°47′4.6″, E110°40′42.3″	quartz (50%) + plagioclase (40%) + K-feldspar (5%) + biotite (5%)
	21LDT-2-01	granodiorite	N25°47′16.2″, E110°40′37.2″	quartz (40%) + plagioclase (20%) + K-feldspar (20%) + biotite (20%)
	21LDT-2-02	granodiorite	N25°47′14.4″, E110°40′37.3″	quartz (45%) + K-feldspar (30%) + plagioclase (15%–20%) + biotite (5%–10%)
Damingshan	21DMS-1	volcanic breccia	N23°23′04″, E108°28′01″	detritus (60%): quartz (70%) + plagioclase (20%) + biotite (10%); matrix (40%): quartz + sericite
	21DMS-2	volcanic breccia		detritus (50%): quartz (50%) + biotite (10%) + calcite (20%) + feldspar (20%); matrix (50%): quartz + calcite + sericite
	21DMS-4	volcanic breccia		detritus (70%): quartz (90%) + feldspar (5%) + muscovite (5%) + detritus (<1%); matrix (30%): quartz + sericite

Zhang W. L. et al., 2017; Chen et al., 2018) for the Early Paleozoic and Early Mesozoic granites in the study area. Despite numerous studies are available, disputes still exit and further work is needed to refine the tecno-thermal evolution and tectonic setting.

The granodiorite samples (21LDT-1, 21LDT-2-01, and 21LDT-2-02) were collected from south of the Yuechengling pluton (Figure 2A), which have typical granitic textures (Figure 3). These rocks consist mainly

FIGURE 3
Field, Hand specimen and microscopic photographs of the Yuechengling granitoids **(A—I)** and the Damingshan volcaniclastic rocks **(J—O)**. Abbreviations: Qtz-quartz, Pl-plagioclase, Kfs-K-feldspar, Bt-biotite, Mic-microcline, Chl-chlorite, Ser-sericite, Amp-amphibole, Fsp-feldspar.

of quartz, plagioclase, K-feldspar, and biotite, while the accessory minerals are mainly magnetite and apatite (Figure 3; Table 1). They have experienced variable degrees of alteration, and exhibit kaolinization and chloritization of K-feldspar and biotite, and sericitization of plagioclase, respectively (Figure 3).

2.2 The Damingshan pluton

The Damingshan pluton is located in the southeastern margin of Youjiang rift basin, central Guangxi Province. The NW-SE trending Nandan-Binyang fault is the main fault, which passes across the Damingshan composite anticline from northwest to southeast. The strata outcropped are from Cambrian (Є) to Quaternary (Q), with Silurian (S) and Jurassic (J) are missing (Figure 2B). Ordovician distributed in the southwest of the Damingshan anticline in an NW-trending strip (Figure 2B), with lithology of greywacke, shale, mudstone, pyroclastic rock, etc., and shows parallel unconformity with the underlying Cambrian strata and angular unconformity with the overlaying Devonian strata. Ordovician only outcropped at the Huang'ai formation (O1h), which distributed in Longtoushan, Shanglin County. Previous studies for the Damingshan pluton mainly focused on deposits (Cai, 2012; Gan et al., 2022) by using geochronology (Yang et al., 2011) or geochemistry (Zhou, 2020) methods, only a few systematic chronology and geochemistry studies had been conducted on the igneous rocks (Chen, 2018; Wang et al., 2020).

The volcaniclastic samples (21DMS-1, 21DMS-2, and 21DMS-4) were collected from the Ordovician strata. The detritus consists of quartz, feldspar, calcite, biotite, and muscovite, most of the quartz and feldspar minerals have been sericitized (Table 1; Figure 3). The component of the matrix is mainly quartz and sericite, with calcite only appearing in sample 21DMS-2 (Table 1; Figure 3).

3 Analytical methods

Whole-rock major and trace element compositions were determined for the granitoid and volcaniclastic samples. The zircons from these samples were used for laser ablation-inductively coupled plasma-mass spectrometer (LA-ICP-MS) zircon U-Pb dating and multicollector-inductively coupled plasma-mass spectrometer (MC-ICP-MS) zircon Lu-Hf isotope analyses.

Major and trace element compositions were undertaken at Guangxi Key Laboratory of Exploration for Hidden Metallic ore Deposits, Guilin University of Technology. Major element compositions were determined using a ZSX Primus II X-ray fluorescence spectrometer (XRF) and the analytical accuracy was better than 2%. Trace element compositions were determined using an Agilent 7500cx inductively coupled plasma mass spectrometry (ICP-MS) and the analytical accuracy was better than 2%. The analytical procedures have been described by Liu X. J. et al. (2020).

Zircon U-Pb dating and Hf isotope analyses were performed at Guangxi Key Laboratory of Hidden Metal Mineral Exploration at Guilin University of Technology. The instrument used for the zircon U-Pb dating was LA-ICP-MS, with a laser beam spot diameter of 32 μm and a frequency of 6 Hz. To ensure reliability of the analyses and stability of the instruments, standard samples were analyzed before and after each group of analyses, using the American national standard silicate glass NIST610. The external standard 91,500 was analyzed twice before and after each group of eight analyses, and internal standard samples were limited by GJ. The measured data were processed using ICPMSDataCal10.2 software, and the U-Pb harmonic graphs and age-weighted average graphs of

samples were drawn using Isoplot v4.15. The zircon $in situ$ Hf isotope analyses were performed using a high-resolution multi-receiver ICP-MS system equipped with an ESI New Wave 193 Ar F excimer laser. The methods were described by Bouvier et al. (2008). Standard zircon GJ whose $^{176}Hf/^{177}Hf$ value is = 0.282000 ± 50 (2σ) was used for external correction, initial $^{176}Hf/^{177}Hf$ values calculations were based on Lu decay constant of 1.865×10^{-11} yr^{-1} (Scherer et al., 2001). Model ages and $ε_{Hf}(t)$ values were calculated under the supposition that the $^{176}Lu/^{177}Hf$ of average crust is 0.015, the $^{176}Hf/^{177}Hf$ and $^{176}Lu/^{177}Hf$ ratios of chondrite are 0.282772 and 0.0332, and ratios of depleted mantle at the present are 0.28325 and 0.0384, respectively (Blichert Toft and Albarède, 1997; Griffin et al., 2004).

4 Analytical results

4.1 Zircon characteristics and U-Pb dating results

4.1.1 The Yuechengling granitoids

Zircon U-Pb ages were obtained and shown in Supplementary Table S1. Zircon grains of sample 21LDT-1, 21LDT-2–01, and 21LDT-2–02 are mostly shaped in prismatic and euhedral, only a few are irregular anhedral and ellipse shapes, mostly 80–210 μm long and 40–80 μm wide, with length/width ratios of 1:1–4:1. As shown in the cathode luminescence (CL) images (Figures 4A–C), most of the zircon grains display a clear oscillatory zonation, which is typical of magmatic origin zircons.

Twenty-two spot analyses were conducted in sample 21LDT-1 (granodiorite) and the CL images show that most of the zircons have magmatic oscillatory zoning (Figure 4A). 22 zircon grains exhibit Th/U values of > 0.2 and 18 of them display age data with ≥ 90% concordance, giving a weighted mean age of 437.0 ± 2.7 Ma (MSWD = 2.9, Figure 5A). The remaining four concordant grains show older $^{206}Pb/^{238}U$ age of 859–549 Ma (Supplementary Table S1), which are probably inherited or captured zircons.

A total of 17 analyses in sample 21LDT-2-01 (granodiorite) exhibit well-developed magmatic oscillatory zoning (Figure 4B) and show concordant ages with ≥ 90% concordance and Th/U values of > 0.2. Five zircon grains have consistent $^{206}Pb/^{238}U$ ages ranging from 475 Ma to 467 Ma (Supplementary Table S1), with a weighted mean age of 470.7 ± 2.9 Ma (MSWD = 0.62, Figure 5B). 11 zircon grains have younger ages ranging from 431 Ma to 440 Ma, with a weighted mean age of 436.0 ± 1.8 Ma (MSWD = 0.55, Figure 5B). The remaining one inherited zircon grains was formed in Neoproterozoic (754 Ma).

Zircons from sample 21LDT-2-02 (granodiorite) exhibit magmatic oscillatory zoning in CL images (Figure 4C) and Th/U values of > 0.2. 20 zircon grains show concordant ages with ≥90% concordance and 16 of them have consistent $^{206}Pb/^{238}U$ ages ranging from 445 Ma to 436 Ma (Supplementary Table S1), with a weighted mean age of 437.8 ± 1.4 Ma (MSWD = 0.92, Figure 5C). The remaining four zircon grains show older age of 481–462 Ma.

4.1.2 The Damingshan volcaniclastic rocks

Zircon grains in sample 21DMS-1, 21DMS-2, and 21DMS-4 are mostly shaped in irregular anhedral and round-ellipse in shapes. They feature in size of 50–320 μm long and 45–160 μm wide, with
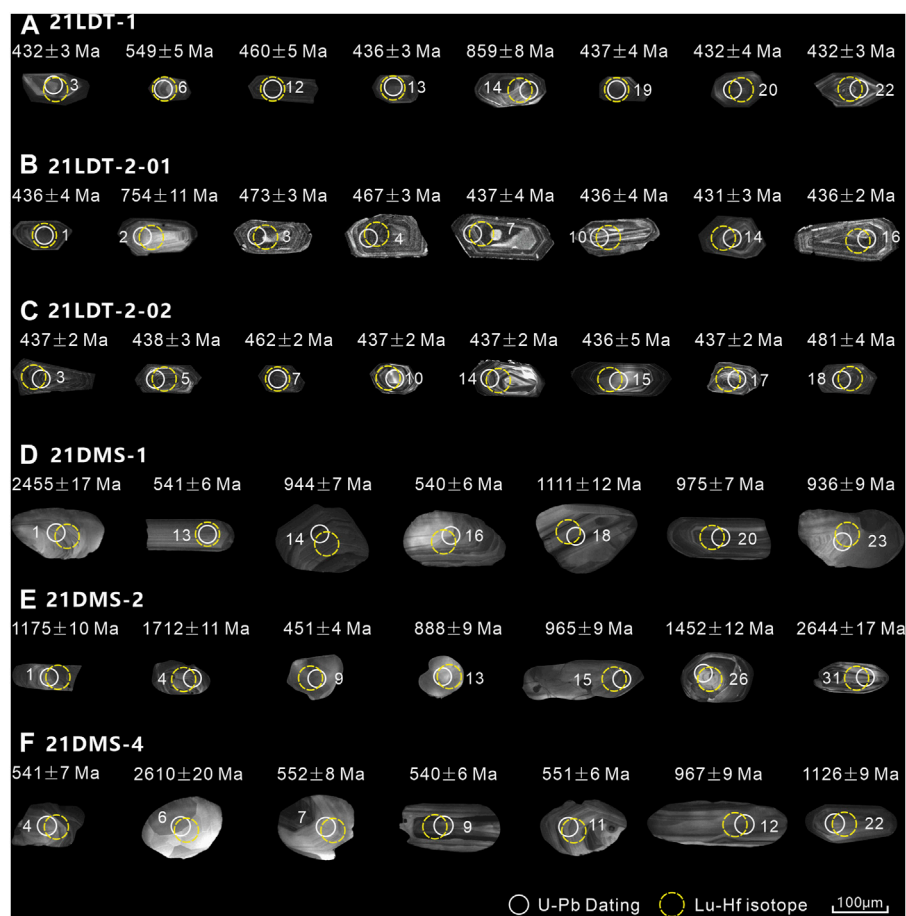
FIGURE 4
Cathode luminescence (CL) images of zircons from the Yuechengling granitoids **(A–C)** and the Damingshan volcaniclastic rocks **(D–F)**.

length/width ratios of 1:1–4:1. As shown in the CL images (Figures 4D–F), most of the zircon grains display a clear oscillatory zonation, which is typical of magmatic origin zircons.

A total of 31 analyses were conducted on zircon grains from sample 21DMS-1 (volcanic breccia), and all have concordant ages with ≥ 90% concordance and Th/U values of > 0.2, defining an age range from 2,478 Ma to 521 Ma (Supplementary Table S1; Figure 5D). These grains define two detrital zircon age modes at ca. 970 Ma and 540 Ma. The oldest zircon grains have an Early Paleoproterozoic age (2,478 Ma) and some detrital zircons define Mesoproterozoic-Neoproterozoic ages (1703–645 Ma). Eight zircons were formed in the Early Paleozoic (542–521 Ma) with the youngest age of 521 ± 6 Ma (96% concordance), which is interpreted to be a maximum depositional age of the rock.

Almost all the 31 zircons in the 21DMS-2 (volcanic breccia) define concordant ages with ≥ 90% concordance. The high Th/U ratios suggest most of magmatic origin. The zircon grains show a wide age range spanning from 2,644 Ma to 451 Ma (Supplementary Table S1; Figure 5E), with a major Neoproterozoic peak (~970 Ma) and minor Early Paleozoic peak (~530 Ma). Three young zircon grains yield Early Paleozoic ages from 543 Ma to 451 Ma, the youngest age of 451 ± 4 Ma (98% concordance) constraining the timing of deposition to be later than 451 Ma.

All of the 24 zircon grains in sample 21DMS-4 (volcanic breccia) show concordant ages with ≥ 90% concordance. The zircon grains also define a broad age ranging from 2,610 Ma to 540 Ma (Supplementary Table S1; Figure 5F) with a peak at ~970 Ma and also carry an Early Paleozoic peak at ~540 Ma. Nine youngest concordant zircons show ages of Early Paleozoic between 552 Ma and 540 Ma with a weighted mean age of 542.7 ± 3.4 Ma (MSWD = 0.57, Figure 5F), suggesting the maximum depositional age.

4.2 Whole-rock major and trace elements

4.2.1 Major elements

Whole-rock major and trace element compositions are presented in Supplementary Table S2.

Granitoids from the Yuechengling pluton have SiO_2 contents of 66.12–67.32 wt%, low $Fe_2O_3^T$ + MgO contents of 5.98–6.31 wt% and $Mg^\#$ values [$Mg^\#$ = atomic Mg/(Mg + Fe)] of 48–49, TiO_2 of 0.45–0.48 wt%, P_2O_5 of 0.11–0.13 wt% and high Al_2O_3 contents of 14.97–16.30 wt%. They have total alkali (ALK = Na_2O+ K_2O) values of 6.10–6.59 wt% and A/CNK [A/CNK = molar Al_2O_3/(CaO + Na_2O+ K_2O)] values of 1.18–1.55 with strongly peraluminous characteristics and plot in the granodiorite and high-K calc-alkaline
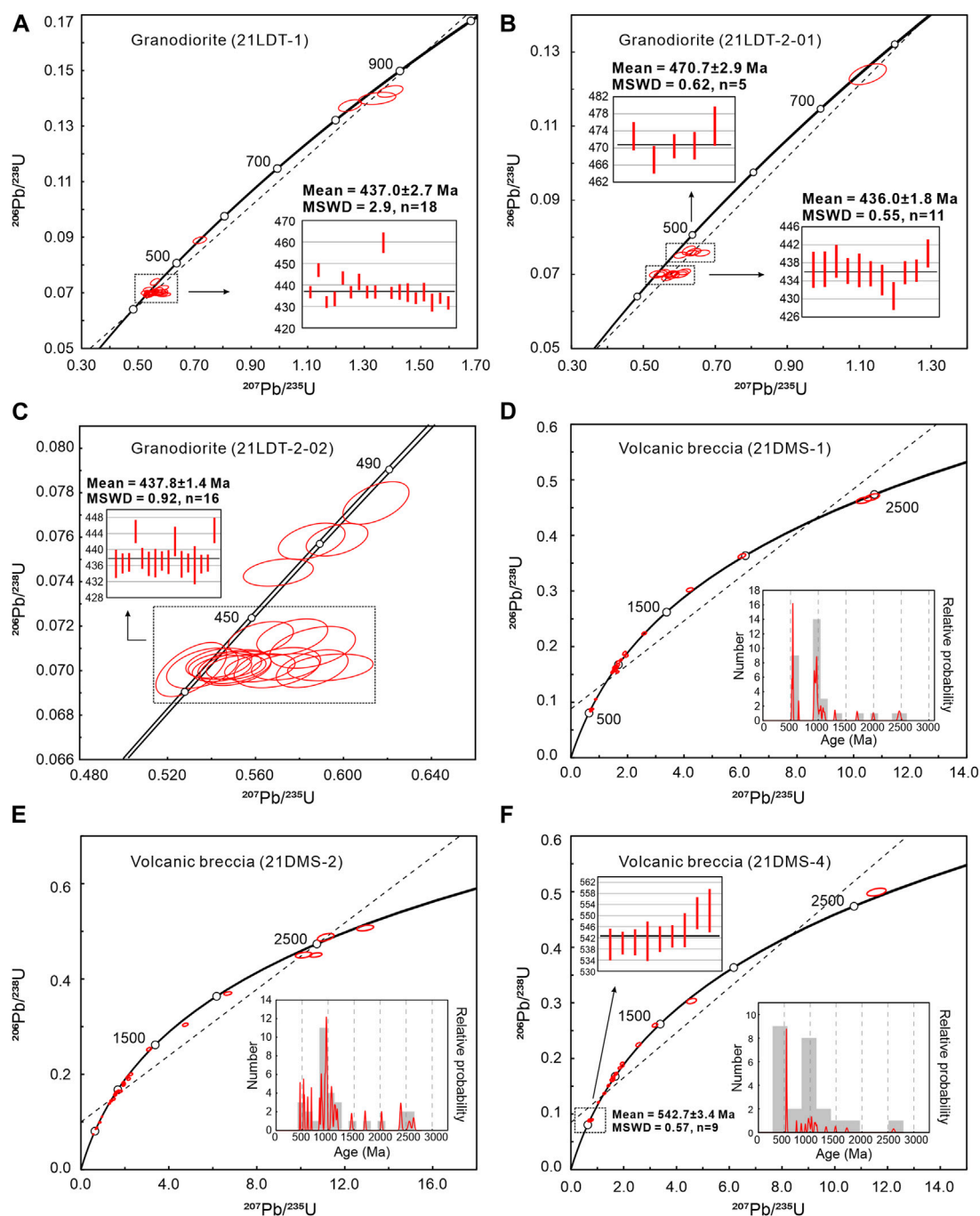
FIGURE 5
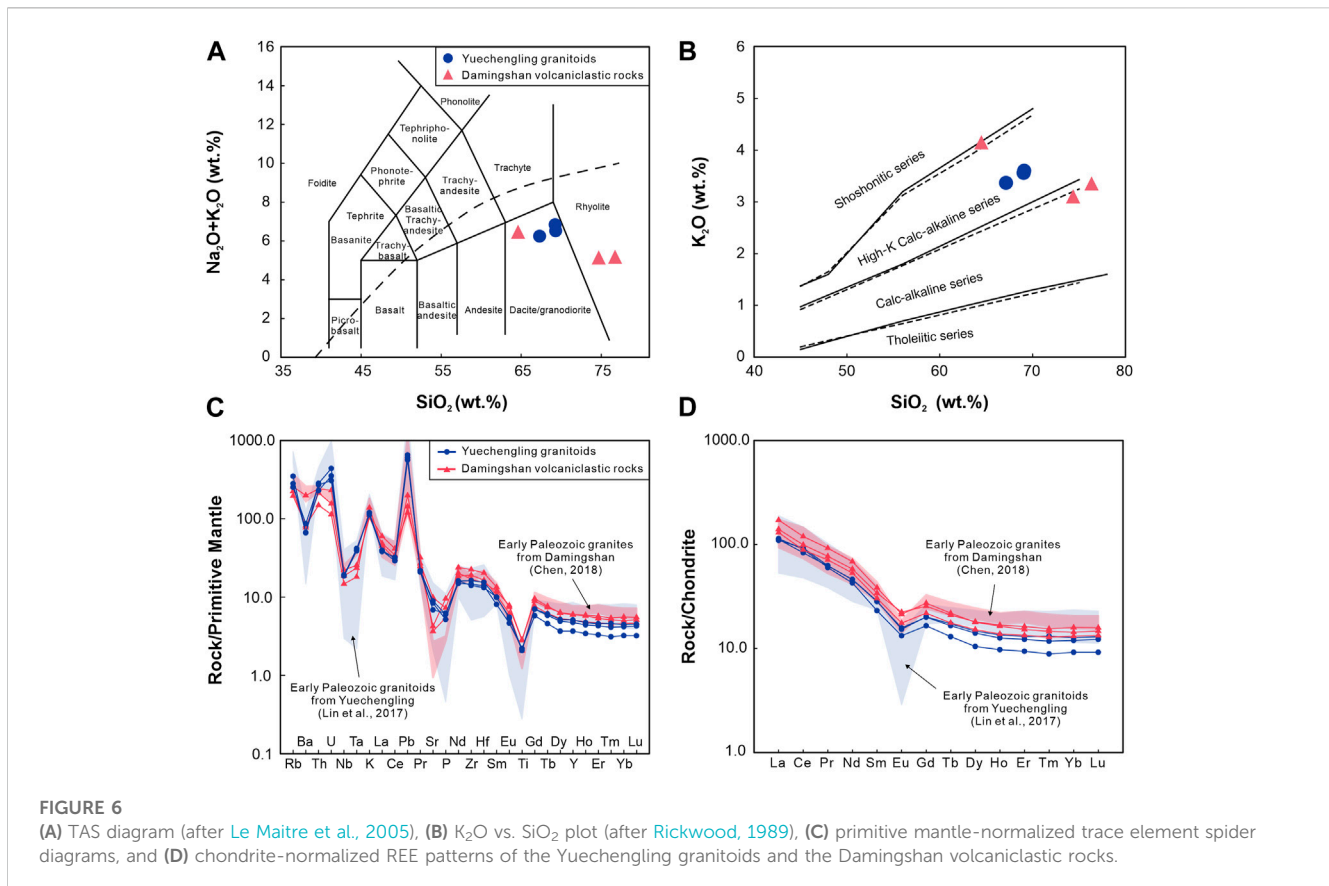Concordant zircon U-Pb dating diagrams of igneous rocks from the Yuechengling pluton **(A–C)** and the Damingshan pluton **(D–F)**.

series fields in the total alkali *vs.* alkali (TAS) and SiO_2 vs. K_2O diagrams (Figures 6A, B). Most of the samples have loss on ignition (L.O.I.) values of <2.5 wt% (1.02–2.44 wt%), indicating weak weathering or secondary alteration.

In contrast, volcaniclastic rocks from the Damingshan pluton have variable SiO_2 contents of 61.23–74.07 wt%, CaO of 0.74–2.91 wt%, $Fe_2O_3^T$ + MgO of 4.34–9.70 wt% and $Mg^\#$ values of 47–56, ALK values of 4.95–6.08 wt%, low TiO_2 of 0.44–0.62 wt% and relatively high Al_2O_3 of 11.44–14.00 wt%. The samples have

relatively high L.O.I. values ranging from 2.46 wt% to 4.77 wt%, probably caused by calcites filled in rock fissures. In the TAS (Figure 6A) and SiO_2 vs. K_2O (Figure 6B) diagrams, the samples fall into the dacite-rhyolite field and show calc-alkaline to high-K calc-alkaline characteristics.

4.2.2 Trace elements

Samples from the Yuechengling and Damingshan plutons have similar trace element compositions, which suggests the similarity of

FIGURE 6
(A) TAS diagram (after Le Maitre et al., 2005), **(B)** K$_2$O vs. SiO$_2$ plot (after Rickwood, 1989), **(C)** primitive mantle-normalized trace element spider diagrams, and **(D)** chondrite-normalized REE patterns of the Yuechengling granitoids and the Damingshan volcaniclastic rocks.

their petrogenesis. In the primitive mantle-normalized trace element spider diagrams (Figure 6C), all the samples show relatively enrichment of large ion lithophile elements (LILEs, e.g., Rb, Th, U, K) and Pb, relative depletion of Ba, Sr, and high field strength elements (HFSEs, e.g., Nb, Ta, P, Ti), and no Zr and Hf anomalies. These features are similar to those of Early Paleozoic granitoids from Yuechengling (Lin et al., 2017).

The samples have total rare Earth element (ΣREE) values of 124–181 ppm, relatively enrichment in light rare Earth elements (LREEs, Figure 6D), and relatively depletion in heavy rare Earth elements (HREEs, Figure 6D), with the LREE/HREE ratios ranging from 7.53 to 10.43 (Supplementary Table S2). The chondrite-normalized REE patterns (Figure 6D) show that the samples have right-inclined HREE patterns, with La$_N$/Yb$_N$ ratios ranging from 8.72 to 12.24, which indicate weak-moderate fractionation between HREEs and LREEs. Besides, the samples exhibit moderate negative Eu anomalies with δEu values of 0.63–0.75 [Figure 6D, Supplementary Table S2, δEu = Eu$_N$/(Sm × Gd)$^{1/2}$], which suggest that there might be plagioclase residue in the source area or its parental magma suffered plagioclase fractionation during its evolution.

4.3 Zircon Lu-Hf isotope

As shown in Supplementary Table S3, *In situ* Lu-Hf isotope analyses of zircons that have ≥ 90% concordance U-Pb ages have been carried out. ^{176}Lu/^{177}Hf ratios of the zircon grains range from 0.000015 to 0.002425. Most of them have ^{176}Lu/^{177}Hf ratios less than

0.002, indicating no accumulation of radiogenic Hf after zircon formation and the ratios of Hf isotopes are not affected by later episodes of partial melting and fractional crystallization, the ratios can essentially represent the Lu-Hf system when the zircon formed (Wu et al., 2007).

4.3.1 The Yuechengling granitoids

Thirteen zircons from sample 21LDT-1 (granodiorite) with concordant ages of 460–432 Ma display uniform (^{176}Lu/^{177}Hf)$_i$ (initial ratio) values of 0.282298–0.282422 (Figure 7A), negative ε$_{Hf}$(t) values ranging from −7.49 to −3.12, and two-stage Hf isotope model ages (T$_{DM2}$) of 1.88–1.60 Ga (Figure 7B). Two inherited or captured zircons with ages of 549 and 859 Ma yielded (^{176}Lu/^{177}Hf)$_i$ values of 0.282414 and 0.281963 (Figure 7A), negative ε$_{Hf}$(t) values of −0.90 and −9.89, T$_{DM2}$ ages of 2.37 and 1.55 Ga (Figure 7B), respectively.

The Lu-Hf analyses were performed on 14 Early Paleozoic (475–431 Ma) zircons from sample 21LDT-2–01 (granodiorite), and these zircons show (^{176}Lu/^{177}Hf)$_i$ values of 0.282278–0.282388 (Figure 7A), corresponding to negative ε$_{Hf}$(t) values of −8.24 to −4.33 and T$_{DM2}$ age of 1.92–1.68 Ga (Figure 7B). The oldest zircon (754 Ma) display relatively high (^{176}Lu/^{177}Hf)$_i$ value of 0.282188 (Figure 7A), negative ε$_{Hf}$(t) value of −4.28, and T$_{DM2}$ age of 1.93 Ga (Figure 7B).

Fifteen zircons from sample 21LDT-2-02 (granodiorite) with the ages of 481–439 Ma were analyzed, results show that they have similar characteristics to the granitoid samples above, which contains (^{176}Lu/^{177}Hf)$_i$ values of 0.282171–0.282379 (Figure 7A)
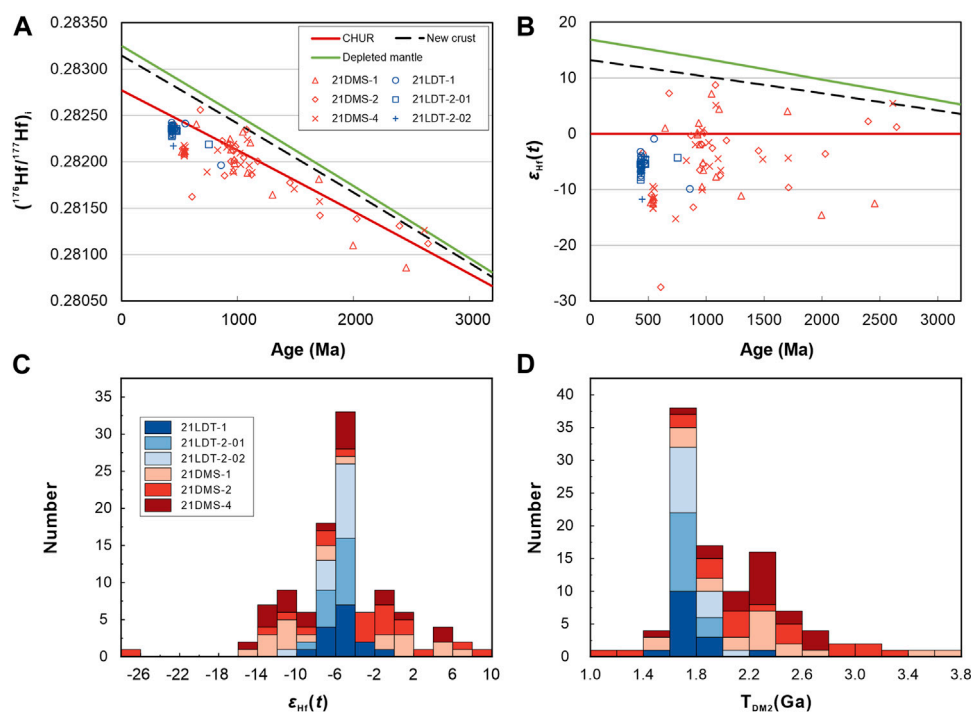
FIGURE 7
Diagrams of Lu-Hf isotopic data for zircons from the Yuechengling granitoids and the Damingshan volcaniclastic rocks. Plots of **(A)** U-Pb ages vs. $(^{176}Lu/^{177}Hf)_i$, **(B)** U-Pb ages vs. $\varepsilon_{Hf}(t)$, Histograms of **(C)** $\varepsilon_{Hf}(t)$ values and **(D)** Hf isotope two-stage model ages.

that correspond to negative $\varepsilon_{Hf}(t)$ values ranging from −11.98 to −4.43 and T_{DM2} ages of 2.16 to 1.70 Ga (Figure 7B).

4.3.2 The Damingshan volcaniclastic rocks

Five zircons with the ages of 542–521 Ma from sample 21DMS-1 (volcanic breccia) show consistent $(^{176}Lu/^{177}Hf)_i$ values ranging from 0.282090 to 0.282125 (Figure 7A), with negative $\varepsilon_{Hf}(t)$ values of −12.53 to −11.27, and T_{DM2} ages of 2.28 to 2.20 Ga (Figure 7B), while 13 Mesoproterozoic-Neoproterozoic (1703–645 Ma) zircons have $(^{176}Lu/^{177}Hf)_i$ values ranging from 0.281646 to 0.282406 (Figure 7A), with both negative and obviously positive $\varepsilon_{Hf}(t)$ values ranging from −11.10 to 7.18, corresponding to variable T_{DM2} ages ranging from 2.79 to 1.43 Ga (Figure 7B). The remaining Early Paleoproterozoic (2,455 Ma) and Late Paleoproterozoic (1996 Ma) zircons have $(^{176}Lu/^{177}Hf)_i$ values of 0.280859 and 0.281099 (Figure 7A), obviously negative $\varepsilon_{Hf}(t)$ values of −12.48 and −14.58, T_{DM2} ages of 3.79 and 3.56 Ga (Figure 7B), respectively.

The youngest (451 Ma) and the other Early Paleozoic (528 Ma) zircons from sample 21DMS-2 (volcanic breccia) display $(^{176}Lu/^{177}Hf)_i$ values of 0.282404–0.282142 (Figure 7A), corresponding to negative $\varepsilon_{Hf}(t)$ values of −3.42 to −10.99 and T_{DM2} ages of 2.17–1.63 Ga (Figure 7B). 15 zircons with Mesoproterozoic-Neoproterozoic ages (1712–608 Ma) yielded higher $(^{176}Lu/^{177}Hf)_i$ values vary from 0.281422 to 0.282561 (Figure 7A), extremely negative to obviously positive $\varepsilon_{Hf}(t)$ values of −27.54 to 8.73, and variable T_{DM2} ages vary from 3.26–1.13 Ga (Figure 7B). The remaining three Neoarchean-Paleoproterozoic zircons with ages from 2,644 Ma to 2028 Ma show a narrow range of $(^{176}Lu/^{177}Hf)_i$

values (0.281118–0.281386) (Figure 7A), corresponding to both negative and positive $\varepsilon_{Hf}(t)$ values of −3.63 to 2.22, and T_{DM2} ages of 3.08–2.82 Ga (Figure 7B).

In sample 21DMS-4 (volcanic breccia), 7 zircons with the ages of 552 Ma to 540 Ma have $(^{176}Lu/^{177}Hf)_i$ values of 0.282065–0.282177 (Figure 7A), obviously negative $\varepsilon_{Hf}(t)$ values of −13.38 to −9.43, and T_{DM2} ages of 2.33–2.08 (Figure 7B), respectively. 12 Mesoproterozoic-Neoproterozoic (1708–737 Ma) zircons exhibit variable $(^{176}Lu/^{177}Hf)_i$ values (0.281573–0.282242) (Figure 7A) that correspond to obviously negative to positive $\varepsilon_{Hf}(t)$ values of −15.26 to 5.08 and variable T_{DM2} ages (2.69–1.59 Ga) (Figure 7B). The oldest zircon with a Neoarchean age of 2,610 Ma shows the lowest $(^{176}Lu/^{177}Hf)_i$ value of 0.281260, corresponding to the highest positive $\varepsilon_{Hf}(t)$ value of 5.45 and the oldest T_{DM2} age of 2.78 Ga (Figure 7B).

5 Discussion

5.1 Formation age of the igneous rocks

Salient information from previous geochronological studies of the Early Paleozoic igneous rocks from the SCB have been reported in the past few years, showing that the igneous rocks were formed between ca. 460 Ma and ca. 390 Ma, and peaked at ca. 440–420 Ma (Li et al., 2011; Wang et al., 2013b; Xin et al., 2020; Kong et al., 2021; Tang et al., 2021 and the related references). Previous studies based on the Early Paleozoic granitoids from the Yuechengling pluton were aged by using LA-ICP-MS zircon U-Pb (Zhao et al., 2013; Chen

et al., 2016; Lin et al., 2017; Chen et al., 2018), zircon SHRIMP U-Pb (Bai et al., 2015), and SIMS zircon U-Pb (Chu et al., 2012) dating methods and obtained age data displaying a wide emplacement age peaked at 435–422 Ma. Our new LA-ICP-MS zircon U-Pb age data further constrain the emplacement age of the granitoids from the Yuechengling pluton to be 438–436 Ma.

In contrast, very few geochronological studies have been conducted for the Early Paleozoic igneous rocks from the Damingshan area, with the reported ages of 441–432 Ma for the granitoids (Chen, 2018; Wang et al., 2020), but a vacancy for the volcaniclastic rocks. In this study, zircons from the volcaniclastic rocks are mainly inherited or captured zircons, and the youngest concordant zircons from three samples are 521 ± 6, 451 ± 4, and 540 ± 6 Ma, respectively. Since the volcaniclastic rocks are commonly deposited soon after a volcanic eruption, its deposited age would be close to the volcanic eruption age. And the volcanic eruption age could be constrained by the youngest group or single igneous zircon age in the volcaniclastic rocks. Consequently, we suggest that the volcaniclastic rocks should be formed by an Early Paleozoic volcanic eruption which is later than 451 Ma. In addition, the inherited zircons from Neoarchean to Neoproterozoic indicated that ancient materials might exist in their source region.

In summary, the emplacement age of the Yuechengling granitoids constrained to be ca. 437 Ma while the deposited age of the Damingshan volcaniclastic rocks to be later than 451 Ma.

5.2 Genetic type of the Yuechengling granitoids

The granites are commonly divided into I-, S-, and A-types according to the nature of protolith and petrographical and geochemical features (Chappell and White, 1974; Loiselle and Wones, 1979). Studies have shown that feldspar is mostly alkali feldspar in A-type granites, often albite-orthoclase solid solutions or intergrowths, and micrographic intergrowths of quartz and alkali feldspars are very common (Collins et al., 1982). However, the Yuechengling granitoids consist of quartz, plagioclase, K-feldspar, biotite, magnetite, and apatite, being inconsistent with the typical petrographic characteristics of A-type granites. Compared with I-type and S-type granites, A-type granites can be distinguished from their high Zr + Nb + Ce + Y contents (average value = 350 ppm) and FeO^T/MgO ratios (average value = 10), and enrichment in HFSEs (e.g., Nb and Ta) (Whalen et al., 1987). Geochemical data of the Yuechengling granitoids display low Zr + Nb + Ce + Y contents (246–275 ppm; average value = 257) and low FeO^T/MgO ratios (1.84–1.93; average value = 1.87) (Supplementary Table S2), lower than the limit and being inconsistent with the Fe-rich characteristics of A-type granites (Whalen et al., 1987). The depletion of HFSEs (Nb, Ta, P, Ti) is also different from typical A-type granites but similar to I- and S-type granites (Figure 6C). Moreover, all the granitoids from this study fall in the range of unfractionated and fractionated I- and S-type granites on the Zr + Nb + Ce + Y vs. FeO^T/MgO (Figure 8A) and Zr + Nb + Ce + Y vs. $(K_2O + Na_2O)/CaO$ diagrams (Figure 8B), which resembles the Yuechengling granitoids reported by Chen et al. (2016), Cheng et al. (2016), and Chen et al. (2018), with only a few samples showing A-type

characteristics which could be produced by strong fractionated S- or I- type granites (Champion and Bultitude, 2013).

I-type and S-type granites have similar mineralogical and geochemical compositions, yet there are some differences. I-type granites contain hornblende and pyroxene, with normative mineral C (Corundum) content of < 1 (Chappell and White, 1974). The granitoids from this study do not have a mineralogy typical of I-type granites, all the studied samples do not contain hornblende or pyroxene with normative mineral C contents of > 1 (2.80–5.87; average value = 3.89). Furthermore, I-type granites are metaluminous to weakly peraluminous (A/CNK value < 1.1) and have relatively high Na_2O contents (>3.2 wt%; Chappell and White, 1992). The studied granitoids are all strongly peraluminous granitoids, with high A/CNK values of 1.18–1.55 (average value = 1.32, with all > 1.1), A/NK values of > 1.0 (1.77–2.00; average value = 1.85), and relatively low Na_2O contents ranging from 2.78 to 3.13 wt% (average value = 2.90 wt%, all < 3.2 wt%; Supplementary Table S2), which are typical characteristics of S-type granites. Moreover, on the SiO_2 vs. $FeO^T/(FeO^T + MgO)$ (Figure 8C) and ACF diagrams (Figure 8D), the granitoids are all distributed in the S-type range, which is similar to previous studies from the Yuechengling pluton, furthering S-type affinity.

5.3 Origin of the Early Paleozoic igneous rocks

5.3.1 The Yuechengling granitoids

S-type granites are usually characterized by felsic compositions with low Fe + Mg contents less than 3%–4% at reasonable crustal pressures and temperatures (Champion and Bultitude, 2013 and references therein), while the Yuechengling granitoids display high-maficity feature with relatively high Fe + Mg contents of 5.98–6.31 wt%. Several different mechanisms of this feature have been proposed, including 1) source heterogeneity, especially heterogeneous continental crustal material sources (e.g., Villaros et al., 2012); 2) magma mixing, incorporation of mantle-derived mafic magma will lead to mafic feature (Clemens et al., 2011; Champion and Bultitude, 2013); 3) selective entrainment of peritectic/restitic and accessory minerals, especially the peritectic garnet (e.g., Zhu et al., 2020; Song and Xu, 2022); 4) hydrothermal alteration, the hydrothermal fluids can bring Fe and Mg components into the granites (e.g., Song and Xu, 2022). Since no peritectic/restitic garnet was contained in the Yuechengling granitoids (Table 1), the mechanism of the entrainment of peritectic garnet was excluded. Thus, a full assessment of the partial melting, source heterogeneity, magma mixing, and fractional crystallization in the magmatic evolution process and the post-magmatic hydrothermal alteration could be accounted for petrogenesis and high-maficity feature of the Yuechengling granitoids.

5.3.1.1 Partial melting and source heterogeneity

Zircon Lu-Hf isotope is of great significance for the study of magmatic evolution and source tracing, since it has extremely high closure temperature, which can maintain primitive Hf isotopic composition even under high-grade metamorphic conditions (Wu et al., 2007). The Yuechengling granitoids have negative $\varepsilon_{Hf}(t)$ values ranging from −11.98 to −0.90, and corresponding
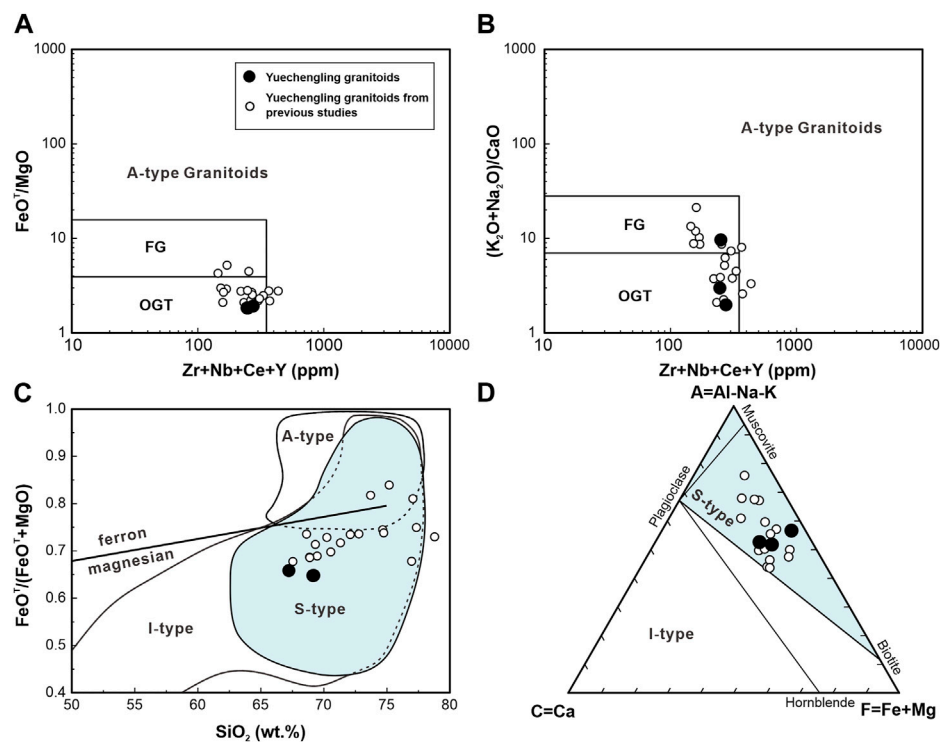
FIGURE 8
Petrogenetic discrimination diagrams of the Yuechengling granitoids: **(A)** Zr + Nb + Ce + Y vs. FeO^T/MgO; **(B)** Zr + Nb + Ce + Y vs. (K$_2$O+ Na$_2$O)/CaO, **(C)** SiO$_2$ vs. FeO^T/(FeO^T + MgO), **(D)** ACF diagram. FG-fractionated M-, I-, and S-type granites; OGT-unfractionated M-, I-, and S-type granites. **(A,B)** are after Whalen et al. (1987), **(C)** is after Frost et al. (2001), **(D)** is after Chappell and White (1992). Previous data of Yuechengling granitoids are from Chen et al. (2016), Cheng et al. (2016), and Chen et al. (2018).

T$_{DM2}$ ages distributed from 2.37 to 1.55 Ga (Figures 7B–D; Supplementary Table S3), indicating that they might be derived from a crustal source of Paleoproterozoic basement. The granitoids have Rb/Sr ratios ranging from 0.95 to 1.25 (average value = 1.1), which are higher than the mantle-derived granitoids (Rb/Sr < 0.05) and crust-mantle-sourced granitoids (Rb/Sr = 0.05–0.50), but consistent with the range of crust-derived granites (Rb/Sr > 0.5; Sylvester, 1998). They have Nb/Ta ratios (7.89–8.4, average = 8.21) that close to the average value of continental crust (Nb/Ta = 11) and significantly less than the average value of primitive mantle (Nb/ Ta = 17.8; Sylvester, 1998). All the granitoids are characterized by depletion of Nb, Ti and enrichment of Pb (Figure 6C), which furthered a crustal source.

There is little controversy about the sources of peraluminous, crustal-evolved, S-type granitic magma, which are derived from partial melting of meta-sedimentary rocks (Clemens et al., 2011). However, some scholars have shown that some S-type granitoids in the SCB are derived from a heterogeneous source (e.g., Zhu et al., 2020). The studied granitoids contained high Al$_2$O$_3$ contents (14.97–16.30 wt%) and show peraluminous characteristics (A/ CNK value = 1.18–1.55, Supplementary Table S2), which can be produced by fractional crystallization of hornblende from subaluminous melts (A/CNK value < 1, Zen, 1986) or partial melting of meta-igneous source rocks (Reichardt and Weinberg, 2012). However, combining with previous studies, the A/CNK values of the Yuechengling granitoids are constant with the

increase of SiO$_2$ contents (Figure 9A) and show negative Eu anomalies (Figure 6D), being inconsistent with fractional crystallization of hornblende from subaluminous melts (Jiang and Zhu, 2017). Moreover, melts produced by partial melting of meta-igneous source rocks usually display enrichments in Na (K$_2$O/ Na$_2$O < 1), Sr (Sr/Rb > 10), and Eu (δEu > 1) (Reichardt and Weinberg, 2012). Our samples contain high K$_2$O/Na$_2$O ratios (1.11–1.26), low Sr/Rb ratios (0.8–1.06) and display depletion in Eu (Supplementary Table S2; Figure 6C), excluding partial melting of meta-igneous source rocks. Generally, melts derived from metapelite show relatively low CaO/Na$_2$O ratios of < 0.3 and metagreywacke-derived melts contain higher CaO/Na$_2$O ratios of 0.3–1.5 (Sylvester, 1998), and granitoids of this study have variable CaO/Na$_2$O ratios of 0.22–1.11. Combining with previous data, on the Rb/Sr vs. CaO/Na$_2$O and Rb/Sr vs. Rb/Ba diagrams (Figures 9C, D), the Yuechengling granitoids are distributed both in the ranges of clay-poor and clay-rich sources, demonstrating the granitoids might be the products of pelite and greywacke melting. In summary, we suggest heterogeneity of meta-sedimentary sources may contribute to the granitoids, and they are derived from a crustal source with both meta-greywacke and meta-pelite components of the ancient basement.

5.3.1.2 Magma mixing and hydrothermal alteration

Recently, a growing number of the Early Paleozoic ultramafic-mafic rocks have been reported in the SCB (e.g., Wang et al., 2013b;
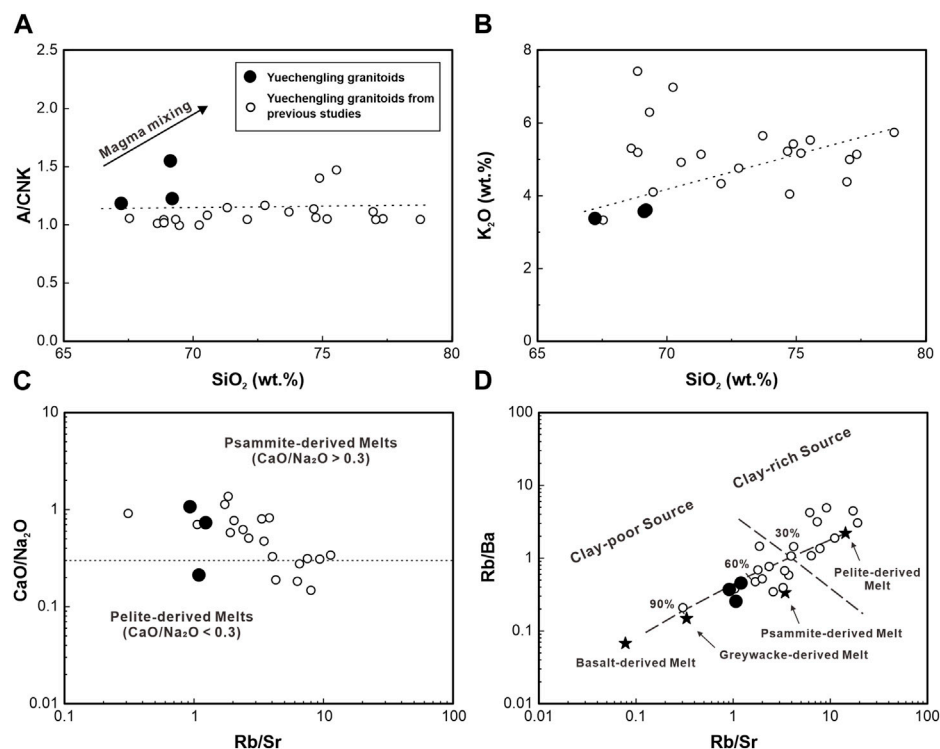
FIGURE 9
Petrogenetic discrimination diagrams of the Yuechengling granitoids. **(A)** SiO$_2$ vs. A/CNK, **(B)** SiO$_2$ vs. K$_2$O, **(C)** Rb/Sr vs. CaO/Na$_2$O, **(D)** Rb/Sr vs. Rb/Ba. **(C)** is after Li et al. (2003), **(D)** is after Sylvester (1998). Previous data of Yuechengling granitoids are from Chen et al. (2016), Cheng et al. (2016), and Chen et al. (2018).

Zhong et al., 2013; 2014; 2016; Zhang et al., 2015), indicating mantal-derived materials involved in generation of the subaluminous felsic magma, and the incorporation of mantle-derived mafic magma will trigger more mafic features such as high ferromagnesian contents of the melts (Clemens et al., 2011). Magma mixing process has been widely discussed on the genesis of the Early Paleozoic granitoids in the SCB, with inputting of mantle-derived materials (e.g., Zhang et al., 2012; Xia et al., 2014; Tang et al., 2021). Generally, variable zircon ε_{Hf}(t) values ranging from negative to positive are considered as a result of mixing between crust-and mantle-derived magma (e.g., Xia et al., 2014). However, the Yuechengling granitoids have negative ε_{Hf}(t) values (−11.98 to −0.90), which indicates that they were derived from a crustal source with no significant mixing between crust- and mantle-derived magma. Granitoids with high Mg$^{\#}$ values (commonly > 50) are possibly having a contribution of mantle-derived components to their parental magma (e.g., Abdallsamed et al., 2017). Samples of this study have Mg$^{\#}$ values of 48–49 (all < 50), furthering no mixing occurred. Moreover, on the SiO$_2$ vs. A/CNK (Figure 9A) diagram, they do not display an obvious trend of magma mixing combining our new data with previous studies. These evidences indicate no certain degree of magma mixing, suggesting that mantle-derived materials were not involved and the model of magma mixing is excluded.

Studies have shown that post-magmatic tectonic-thermal events can lead S-type granites to more mafic features, the hydrothermal

fluids can bring Fe and Mg components into granites (e.g., Song and Xu, 2022). The granitoids from our study exhibit kaolinization and chloritization of K-feldspar and biotite, respectively, accompanied by sericitization of plagioclase. These petrographic characteristics indicate that they have been modified by variable degrees of intermediate- and low-temperature hydrothermal alteration. At the same time, hornblende can retrogress to biotite under hydrothermal conditions, which explains the absence of hornblende in the granodiorite samples. Moreover, most of the deposits in the Yuechengling area are considered related to magmatic-hydrothermal activities (Wu et al., 2012; Chen et al., 2016). Thus, the hydrothermal alteration can be the most reasonable explanation for the high-maficity feature of the granitoids in this paper. It should be noted that the proportion of Mg component in the hydrothermal fluids might be relatively high, by the reason of our samples contain relatively high Mg$^{\#}$ values nearly close to 50 and no mantle-derived materials were involved in their magma source.

However, due to the existence of coetaneous mantle-derived magmatic products in the SCB, the high-maficity feature of the Yuechengling S-type granitoids is attributed to the involvement of mantle-derived materials or the alteration of hydrothermal fluids should be further examined in future studies.

5.3.1.3 Fractional crystallization

On the Zr + Nb + Ce + Y vs. FeO^T/MgO (Figure 8A) and Zr + Nb + Ce + Y *vs.* (K$_2$O+Na$_2$O)/CaO diagrams (Figure 8B), the samples all
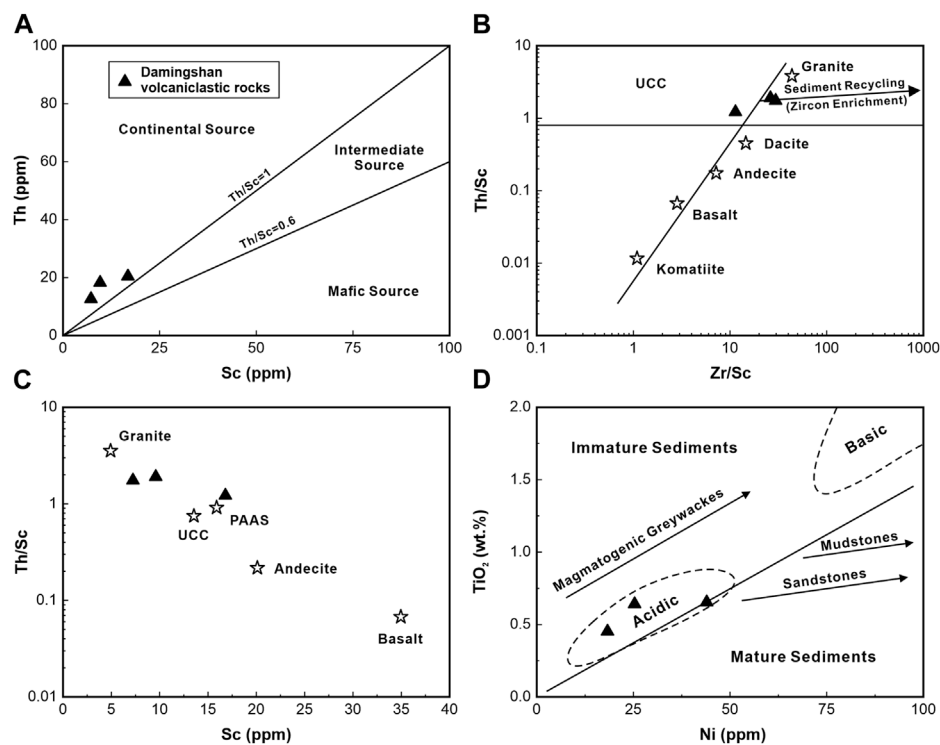
FIGURE 10
Diagrams of **(A)** Sc vs. Th, **(B)** Zr/Sc vs. Th/Sc, **(C)** Sc vs. Th/Sc, and **(D)** Ni vs. TiO$_2$. **(A)** is after Nagarajan et al. (2015), **(B)** is after McLennan et al. (1993), averages of the rocks are after Roser et al. (2002), **(C)** is after Nagarajan et al. (2015), **(D)** is after Floyd et al. (1990). PASS-Post-Archean Australian Shales; UCC-Upper Continental Crust.

fall into the weakly fractionated granitoid field, indicating some degree of fractional crystallization. The granitoids have low contents of SiO$_2$ (66.12–67.32 wt%) and Differentiation index (DI) (73.46–84.96) and ratios of Rb/Sr (0.95–1.25), high ratios of K/Rb (135–184) (Supplementary Table S2), demonstrating a limited fractional crystallization (Sami et al., 2020).

Fractional crystallization or residual of plagioclase can be indicated by depletion of Eu (Figure 6D). Nb and Ti are commonly hosted in Ti-bearing minerals (e.g., ilmenite and titanite), the depletion of Nb and Ti are indicative of the fractional crystallization of Ti-bearing minerals and a crustal magma source (Figure 6C). The depletion of P (Figure 6C) and low contents of P$_2$O$_5$ (0.11–0.13 wt%, Supplementary Table S2) are related to fractionation of apatite (Healy et al., 2004). Moreover, the increases in K$_2$O contents with increasing SiO$_2$ contents show that there was no obvious fractional crystallization of K-feldspar and biotite (Figure 9B). Therefore, the Yuechengling granitoids have undergone some degree of fractional crystallization of plagioclase, Ti-bearing minerals, and apatite.

5.3.2 The Damingshan volcaniclastic rocks
5.3.2.1 Weathering and sediment recycling.

The chemical index of alteration (CIA) [CIA = molar Al$_2$O$_3$/(Al$_2$O$_3$ + CaO* + Na$_2$O + K$_2$O) × 100] is often used as an important parameter to reveal weathering degree of source rocks (Nesbitt and Young, 1982). Generally, rocks with CIA values of 45–55 show low

degree of weathering (CIA of the crust is ca. 47) and value of 100 to be intense degree of weathering, with the alkali and alkaline Earth elements no longer retained (McLennan et al., 1993). The Damingshan volcaniclastic rocks have CIA values ranging from 52 to 61 with an average value of 57 (Supplementary Table S2), indicating incipient weathering conditions. These rocks have maturity index Al$_2$O$_3$/(Na$_2$O + K$_2$O) values of limited variation of 2.30–2.44, showing similar and low maturity and proximal sources.

Th and Zr are incompatible elements in the symbiotic components of igneous rocks and are often enriched in felsic rocks, whereas Sc often contained as a compatible element in the mafic mineral components in the initial stage of magmatic evolution (McLennan and Taylor, 1991). The ratio of Th/Sc is considered to be an indicator of revealing average provenance and enrichment degree of zircon (heavy-mineral), which will increase with the sediment recycling process (McLennan et al., 1993). In the Zr/Sc vs. Th/Sc diagram (Figure 10B), the volcaniclastic rocks are distributed along the compositional variation trend, indicating a low degree of sediment recycling and heavy-mineral sorting. Thus, the geochemistry data of the volcaniclastic rocks are valid for further discussion.

5.3.2.2 Provenance

For clastic sedimentary rocks that have not undergone significant sediment recycling, their geochemistry

characteristics can be used for distinguishing between mafic/ultramafic and felsic source materials (Taylor and McLennan, 1985; Wronkiewicz and Condie, 1987). Al_2O_3/TiO_2 ratios could be used to discriminate the characteristics of source rocks, with mafic rocks having low Al_2O_3/TiO_2 ratios of 3-8, intermediate rocks of 8–21 and felsic rocks of higher ratios (21–70) (Hayashi et al., 1997). Volcaniclastic rocks of this study have relatively high Al_2O_3/TiO_2 ratios of 19.4–26.1, suggesting intermediate to felsic components in the source area. On the Th vs. Sc plot, the rocks concentrate in the field of continental sources (Figure 10A). On the Th/Sc vs. Zr/Sc diagram (Figure 10B), the samples distributed between the dacite and granite fields. On the Sc vs. Th/Sc diagram (Figure 10C), they concentrate between andesite and granite which are closer to granite field. Combining with Ni vs. TiO_2 diagram (Figure 10D), the rocks were suggested to be acidic rather than mafic. The REE contents and Eu anomalies of clastic sedimentary rocks are also important keys for source rock characteristics (Xiang et al., 2015). Mafic rocks have lower LREE/HREE ratios and no negative Eu anomalies, whereas felsic rocks generally have higher LREE/HREE ratios and negative Eu anomalies (Yan et al., 2012). The samples have relatively high LREE/HREE ratios ranging from 7.53 to 9.12 with average value of 8.27 (Supplementary Table S2), and exhibit moderate negative Eu anomalies (Figure 6D), also indicating mainly felsic sources. The plots are consistent with the interpretation that the principal source rocks were of felsic composition with some intermediate composition included. The inference is also supported by mineral assemblages (Table 1; Figure 3).

Zircon grains from our samples exhibit mostly negative $\varepsilon_{Hf}(t)$ values with partially positive (−27.54 to 8.73, Figures 7B, C), indicating that they were dominantly derived from crustal material and may have undergone some degree of magma mixing with mantle-derived materials. Moreover, the relatively high Mg# values (47–56, Supplementary Table S2) of the samples also indicate the contribution of mantle-derived components. Zircons with negative $\varepsilon_{Hf}(t)$ values (−27.54 to −0.14) show T_{DM2} ages of 3.79 to 1.63 Ga, suggesting that they were mainly derived from Archean-Mesoproterozoic crustal materials. Therefore, combined with petrographic and geochemical data, we suggest that the felsic parental magma was erupted to the surface in a Late Ordovician volcanic event (later than 451 Ma) and deposited soon after the eruption.

5.4 Constraints on the Early Paleozoic tectonic evolution of the SCB

Controversy surrounds the tectonic evolution of the Early Paleozoic orogeny in the SCB and two disparate tectonic models have been presented: 1) intracontinental orogeny (Charvet et al., 2010; Xia et al., 2014; Shu et al., 2015; Faure et al., 2017; Tang et al., 2021), i.e., the Yangtze and Cathaysia Blocks were amalgamated together into the ancient South China continent during the amalgamation process of the Rodinia supercontinent in the Late Neoproterozoic, and the Early Paleozoic "Huanan Ocean" did not exist. 2) oceanic subduction-collision (Qin et al., 2011; Peng et al., 2016a;

Peng et al., 2016b; Liu et al., 2018), i.e., the "Huanan Ocean" existed and oceanic subduction occurred in the SCB in the Early Paleozoic.

As absence of the Early Paleozoic ophiolites, island arc igneous rock, coeval HP/LT (high pressure-low temperature)-type metamorphic rocks and turbidite with "Bouma sequence" related to closure of the "Huanan Ocean" are lacking in the SCB, the intra-continental orogenic model has been widely accepted (e.g., Charvet et al., 2010; Wang et al., 2011; Shu et al., 2014). Meanwhile, some "Early Paleozoic island arc igneous rock" and "ophiolite suites" from the southwest segment of the Jiangnan Orogen have been reported recently. Based on geochemical, petrological and geochronological studies, the existence of the Early Paleozoic "Huanan Ocean" and several different subductional-collisional models have been proposed (Peng et al., 2016a; Peng et al., 2016b; Qin et al., 2017). However, the origin of igneous rock with subductional signature is uncertain. The Early Paleozoic igneous rocks in the SCB generally show depletion of HFSEs (e.g., Nb and Ta), which is geochemically similar to island arc magma, and were considered to be formed in a subductional-collisional setting (Qin et al., 2011; Qin et al., 2017). However, the interpretation of "subductional signature" is not only applied to island arc magma. In some cases, the depletion of Nb and Ta can be caused by some magmatism related to intra-plate rift (Rudnick and Gao, 2003; Murphy and Dostal, 2007), or magma derived from the melting of ancient island arc material (Li et al., 2005), lithosphere mantle, or contamination of crustal materials (Zhang X. S. et al., 2017). Furthermore, the complete sequence and age of the Early Paleozoic "ophiolite suit" are uncertain. Although a suit of the Early Paleozoic "ophiolite" was found in the Nuodong area of the SCB (Peng et al., 2016a), it lacks the ultramafic rock (mantle peridotite) unit and should be excluded from the standard ophiolite suit. In addition, some "Early Paleozoic ophiolite" in the SCB was confirmed to be formed in Neoproterozoic (Li et al., 2005; Shu et al., 2006). Thus, further work is needed to refine the integrity and age of the "ophiolite suit".

Igneous rocks formed in the subductional-collisional setting generally display a linear distribution (Zhang et al., 2013). Compared with the Late Mesozoic granites in the SCB (Li and Li, 2007), the spatial and temporal distribution of the Early Paleozoic granites does not display a clear trend of gradually younger age from inland to coastal caused by the plate retracement (Liu X. et al., 2020). From southeast to northwest, the SCB displays uninterrupted detrital zircon ages and sedimentary facies of the Lower Paleozoic sedimentary rocks (Wang et al., 2010; Yu et al., 2015). Combining with biostratigraphy, paleocurrent, and paleoecology signature (Chen et al., 2010; Shu et al., 2014; Yu et al., 2015), it is suggested that the Yangtze and Cathaysia Blocks were not separated in the Early Paleozoic.

Moreover, there is no sufficient geochemical evidence for the existence of asthenosphere mantle-derived igneous rock. The Early Paleozoic mafic igneous rocks reported in the SCB are characterized by extremely low $\varepsilon_{Hf}(t)$ and $\varepsilon_{Nd}(t)$ values and show depletions in HFSEs (e.g., Nb and Ta), which is similar to igneous rocks of the lithospheric mantle source (Jia et al., 2017). Therefore, the Yuechengling granitoids and Damingshan volcaniclastic rocks were probably formed in an intra-continental setting rather than a subductional-collisional setting.
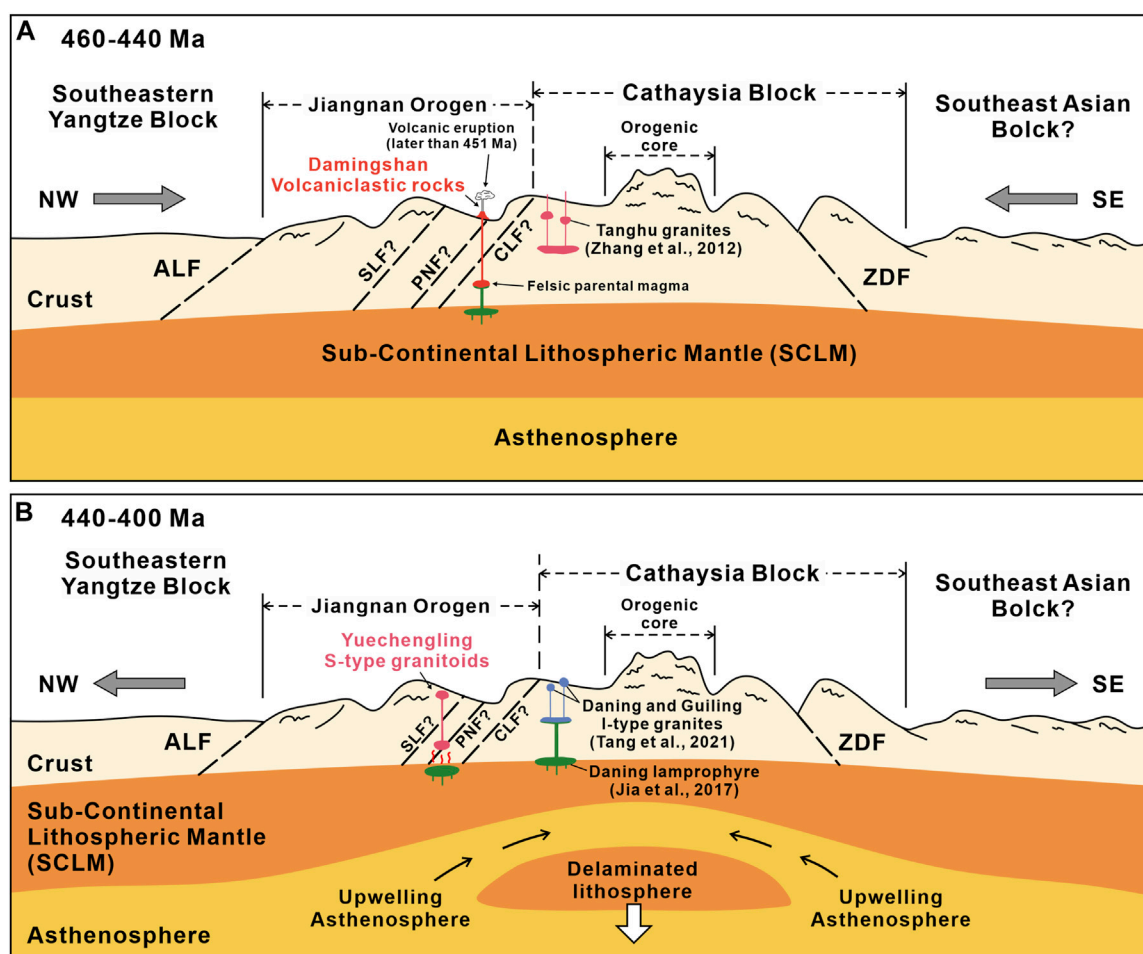
FIGURE 11
Cartoon showing the petrogenetic mechanisms that led to the formation of the Early Paleozoic igneous rocks in the SCB during **(A)** 460 to 440 Ma and **(B)** 440 to 400 Ma (modified after Tang et al., 2021 and Yao et al., 2012). ALF-the Anhua-Luocheng fault, CLF-the Chenzhou-Linwu fault (after Zhao, 2015), PNF-the Pingxiang-Gongcheng-Nanning fault (after Zhou and Wen, 2021), SLF-the Shizong-Mile-Luodian fault (after Dong et al., 2015), ZDF-the Zhenghe-Dapu fault.

According to the currently chronological data from the SCB, the Early Paleozoic orogeny in the SCB started in the Late Ordovician (ca. 460 Ma), peaked at the Early-Mid Silurian (ca. 440–420 Ma), and ended in the Early Devonian (ca. 390 Ma) (Li et al., 2011; Wang et al., 2013b; Xin et al., 2020; Kong et al., 2021; Tang et al., 2021 and the related references). It has been accepted that the Early Paleozoic orogeny has undergone two episodes of tectonic stages, including the syn-collisional stage (ca. 460–440 Ma) and post-collisional stage (ca. 440–400 Ma) (Xia et al., 2014; Yu et al., 2016; Cai et al., 2017; Tang et al., 2021).

Generally, the tectonic setting of granites and intermediate rocks has uncertainty, they can be formed in a compressional setting as well as an extensional setting (except for A-type granites). However, peraluminous S-type granites are generally found in settings associated with the syn-collisional or post-collisional stage (Kalsbeek et al., 2001; Atherton and Ghani, 2002). Generally, thickening of the crust, detachment of the subducted slab (Atherton and Ghani, 2002) and lithospheric delamination (Sylvester, 1998) are some of the mechanisms envisaged for the

heat source that led to partial melting of sedimentary rocks to generate S-type granites. In contrast, ultramafic-mafic rocks are normally considered as products of a regional extensional setting, which are important manifestation of deep thermal-dynamic action on the surface. Recently, some mafic-intermediate rocks in the SCB have been reported, such as the Northern Guangdong high-magnesian andesites and dacites (ca. 435 Ma) (Yao et al., 2012), Longhugang (423 ± 8 Ma), Xinchuan (434 ± 6 Ma) and Xinsi (420 ± 3 Ma) gabbroic plutons (Wang et al., 2013b), Dakang gabbroic pluton (441.1 ± 4.7 Ma) (Zhang et al., 2015), Taoyuan hornblende gabbro (409 ± 2 Ma) (Zhong et al., 2013), and Daning lamprophyre (445 ± 4 Ma) (Jia et al., 2017). A-type granites related to extensional setting are also found in the SCB, such as the South Fufang and Yingshang granitoids (ca. 414–404 Ma) (Xin et al., 2020), Xiqin granites (410 Ma) (Cai et al., 2017), Huitong and Epo granites (414–415 Ma) (Feng et al., 2014). Thus, the tectonic setting of the Early Paleozoic orogeny was changed to a strongly extensional environment at least since ca. 445 Ma, and the timing of tectonic transition

might be further constrained to 445–440 Ma based on these Early Paleozoic ultramafic-mafic rocks and A-type granites in the SCB. It is suggested that the Damingshan volcaniclastic rocks (later than 451 Ma) might be formed in the syn-collisional stage while the Yuechengling granitoids (~437 Ma) in the post-collisional stage.

Crustal shortening, deep metamorphism, crustal collapse and extension should be involved in an orogenic cycle (Froidevaux and Ricard, 1987). Recently, a model of the Early Paleozoic magmatic activity in the SCB was related to the partially molten SCLM heated by upwelling asthenosphere triggered by lithospheric delamination is proposed (e.g., Yao et al., 2012; Wang et al., 2013b; Zhang et al., 2015; Jia et al., 2017). The Early Paleozoic volcanic and mafic rocks are rarely reported compared to granites in response to the synchronous Early Paleozoic orogeny (Wang et al., 2013b), which is similar with areas suspected to have undergone recent delamination that characterized by insignificant mafic magmatism (Ducea, 2011). And that may be due to the formation of extensive intra-crustal felsic magma and the thick Cambrian-Ordovician strata in the SCB, which acted as barriers against the rise of mafic magma (Xu and Xu, 2015). Moreover, the melting temperature for the basaltic magma and the calculated mantle potential temperature are both ca. 1,300°C, similar to that of a MORB (Mid Ocean Ridge Basalt)-like asthenospheric mantle (Yao et al., 2012), supporting the hypothesis that the partially molten SCLM was heated up by upwelling asthenosphere triggered by dropping of the delaminated lithosphere.

Based on previous studies and this study, the Early Paleozoic tectonic evolution process in the SCB is as follows:

(1) From 460 to 440 Ma (Figure 11A), the SCB has undergone crustal shortening and crustal thickening, leading to a peak metamorphic pressure of >8 GPa and temperature of 835°C–878°C with a series of thrust faults developed (Yu et al., 2003; 2007; Li et al., 2010; Xia et al., 2014). The induced metamorphism caused melting of meta-sedimentary rocks in the crust and formed the parental magma after some degree of magma mixing. Subsequently, formation of the thrust faults provided magma conduits for intrusion or eruption of the parental magma, the syn-collisional igneous rocks were formed (e.g., Tanghu granites, Zhang et al., 2012, and the Damingshan volcaniclastic rocks in this study).

(2) From 440 to 400 Ma (Figure 11B), the orogen gradually transforms from compression to extension. After peak metamorphism and exhumation, the extension led the metamorphism to an isothermal metamorphic temperature and decreasing pressure of ca. 4 GPa (Li et al., 2010). Due to the decreasing metamorphic pressure, the SCLM have undergone delamination with rapid unroofing and collapsing, and leading to upwelling of the asthenosphere, which input thermal for partial melting of the SCLM above (Li et al., 2010; Yao et al., 2012; Wang et al., 2013b; Xia et al., 2014). The basaltic magma formed by the partially molten SCLM underplated the crust (e.g., Jia et al., 2017), causing partial melting of the meta-sedimentary rocks to form the felsic magma. At this stage, parental magmas of some granites were formed in the interaction of the basaltic and felsic magma (e.g., Daning and Guiling granites, Tang et al., 2021). After undergoing some degree of assimilation fractional crystallization, the post-collision igneous rocks were produced

(the Yuechengling granitoids in this study). Accompanied by cooling retrogression, the orogen gradually adjusted to the normal crustal thickness, and the Early Paleozoic orogeny ended in the Early Devonian (ca. 400–390 Ma).

6 Conclusion

(1) The Yuechengling granitoids (438–436 Ma) are S-type granitoids. Their parental magma was derived from a crustal meta-greywacke and meta-pelite components in the Paleoproterozoic basement, and have undergone some degree of fractional crystallization.

(2) The Damingshan volcaniclastic rocks (later than 451 Ma) are classified as strongly peraluminous, calc-alkaline to high-K calc-alkaline volcaniclastic rocks. Their parental magma was derived from Neoarchean-Neoproterozoic crustal materials, and has undergone some degree of magma mixing with mantle-derived magma. The felsic parental magma was erupted to the surface in a Late Ordovician volcanic event (later than 451 Ma) and deposited soon after the eruption.

(3) Combining with the previous studies and our new evidence on the Early Paleozoic igneous rock in the SCB, we suggest that the Early Paleozoic tectonic setting of the SCB was intracontinental orogeny rather than oceanic subduction-collision. Granitoids and volcaniclastic rocks in this study recorded the transitional stage of syn-collision compressional (ca. 460–440 Ma) and the post-collision extensional setting (ca. 440–400 Ma) of the Early Paleozoic orogeny.

Data availability statement

The original contributions presented in the study are included in the article/Supplementary Material, further inquiries can be directed to the corresponding author.

Author contributions

YT: writing-original draft, methodology. YS: supervision, conceptualization, reviewing, and editing manuscript. BW, YZ, and YL: experiment assistance, data curation. All authors contributed to the article and approved the submitted version.

Funding

Acknowledgments

Conflict of interest

The authors declare that the research was conducted in the absence of any commercial or financial relationships that could be construed as a potential conflict of interest.

Publisher's note

All claims expressed in this article are solely those of the authors and do not necessarily represent those of their affiliated organizations, or those of the publisher, the editors and the reviewers. Any product that may be evaluated in this article, or claim that may be made by its manufacturer, is not guaranteed or endorsed by the publisher.

Supplementary material

The Supplementary Material for this article can be found online at: https://www.frontiersin.org/articles/10.3389/feart.2023.1202477/full#supplementary-material

References

Abdallsamed, M. I. M., Wu, Y.-B., Zhang, W., Zhou, G., Wang, H., and Yang, S. (2017). Early Paleozoic high-Mg granodiorite from the Erlangping unit, North Qinling orogen, central China: Partial melting of metasomatic mantle during the initial back-arc opening. *Lithos* 288-289, 282–294. doi:10.1016/j.lithos.2017.07.016

Atherton, M. P., and Ghani, A. A. (2002). Slab breakoff: A model for caledonian, late granite syn-collisional magmatism in the orthotectonic (metamorphic) zone of scotland and donegal, Ireland. *Lithos* 62 (3), 65–85. doi:10.1016/S0024-4937(02)00111-1

Bai, D. Y., Zhong, X., Jia, P. Y., Xiong, X., and Huang, W. Y. (2015). The zircon SHRIMP U-Pb dating, geochemical characteristics and tectonic setting of Caledonian Yuechengling pluton in the Western segment of the Nanling Mountains. *Geochimica* 44 (1), 27–42. (in Chinese with English Abstract). doi:10.19700/j.0379-1726.2015.01.003

Blichert Toft, J., and Albarède, F. (1997). The Lu-Hf isotope geochemistry of chondrites and the evolution of the mantle-crust system. *Earth Planet. Sci. Lett.* 148 (1), 243–258. doi:10.1016/S0012-821X(97)00040-X

Bouvier, A., Vervoort, J. D., and Patchett, P. J. (2008). The Lu–Hf and Sm–Nd isotopic composition of CHUR: Constraints from unequilibrated chondrites and implications for the bulk composition of terrestrial planets. *Earth Planet. Sci. Lett.* 273 (1), 48–57. doi:10.1016/j.epsl.2008.06.010

Cai, D. W., Tang, Y., Zhang, H., Lv, Z. H., and Liu, Y. L. (2017). Petrogenesis and tectonic setting of the devonian Xiqin A-type granite in the northeastern Cathaysia block, SE China. *J. Asian Earth Sci.* 141, 43–58. doi:10.1016/j.jseaes.2016.05.015

Cai, H. Q. (2012). Geological characteristics of Damingshan tungsten polymetallic deposit in Guangxi and its exploration prospect. *Mineral Resour. Geol.* 26 (3), 205–209. (in Chinese with English Abstract). doi:10.3969/j.issn.1001-5663.2012.03.006

Champion, D. C., and Bultitude, R. J. (2013). The geochemical and SrNd isotopic characteristics of Paleozoic fractionated S-types granites of north Queensland: Implications for S-type granite petrogenesis. *Lithos* 162-163, 37–56. doi:10.1016/j.lithos.2012.11.022

Chappell, B. W., and White, A. J. R. (1992). I- and S-type granites in the lachlan fold belt. *Earth Environ. Sci. Trans. R. Soc. Edinb.* 83 (1-2), 1–26. doi:10.1017/S0263593300007720

Chappell, B. W., and White, A. J. R. (1974). Two contrasting granite types. *Pacif. Geol.* 8, 173–174.

Charvet, J., Shu, L. S., Faure, M., Choulet, F., Wang, B., Lu, H. F., et al. (2010). Structural development of the lower paleozoic belt of south China: Genesis of an intracontinental orogen. *J. Asian Earth Sci.* 39 (4), 309–330. doi:10.1016/j.jseaes.2010.03.006

Charvet, J., Shu, L. S., Shi, Y. S., Guo, L. Z., and Faure, M. (1996). The building of south China: Collision of yangzi and Cathaysia blocks, problems and tentative answers. *J. Southeast Asian Earth Sci.* 13 (3), 223–235. doi:10.1016/0743-9547(96)00029-3

Charvet, J. (2013). The neoproterozoic–early paleozoic tectonic evolution of the South China block: An overview. *J. Asian Earth Sci.* 74, 198–209. doi:10.1016/j.jseaes.2013.02.015

Chen, J. H. (2018). *Geochemical characteristics and petrogenesis of the caledonian granite in southwestern south China block*. Beijing): China University of Geosciences. Master.

Chen, W. D., Zhang, W. L., Wang, R. C., Chu, Z. Y., Xiao, R., Zhang, D., et al. (2016). A study on the Dushiling tungsten-copper deposit in the Miao'ershan-Yuechengling area, Northern Guangxi, China: Implications for variations in the mineralization of multi-aged composite granite plutons. *Sci. China (Earth Sci.* 59 (11), 2121–2141. doi:10.1007/s11430-015-5360-3

Chen, X. L., Liang, H. Y., Richards, J. P., Huang, W. T., Zhang, J., Wu, J., et al. (2018). Age and granite association of skarn W mineralization at Niutangjie district, South China Block. *Ore Geol. Rev.* 102, 268–283. doi:10.1016/j.oregeorev.2018.09.003

Chen, X., Zhang, Y. D., Fan, J. X., Cheng, J. F., and Li, Q. J. (2010). Ordovician graptolite-bearing strata in southern Jiangxi with a special reference to the Kwangsian Orogeny. *Sci. China Earth Sci.* 53 (11), 1602–1610. doi:10.1007/s11430-010-4117-6

Cheng, S. B., Fu, J. M., Ma, L. Y., Lu, Y. Y., Kou, X. H., Zhang, L. G., et al. (2016). Origin of the yuechengling caledonian granitic batholith, northeastern Guangxi: Constraint from zircon U-Pb geochronology, geochemistry and Nd-Hf isotopes. *Geotect. Metallogenia* 40 (4), 853–872. (in Chinese with English Abstract). doi:10.16539/j.ddgzyckx.2016.04.017

Chu, Y., Lin, W., Faure, M., Wang, Q. C., and Ji, W. B. (2012). Phanerozoic tectonothermal events of the Xuefengshan Belt, central South China: Implications from U-Pb age and Lu-Hf determinations of granites. *Lithos* 150, 243–255. doi:10.1016/j.lithos.2012.04.005

Clemens, J. D., Stevens, G., and Farina, F. (2011). The enigmatic sources of I-type granites: The peritectic connexion. *Lithos* 126 (3), 174–181. doi:10.1016/j.lithos.2011.07.004

Collins, W. J., Beams, S. D., White, A. J. R., and Chappell, B. W. (1982). Nature and origin of A-type granites with particular reference to southeastern Australia. *Contributions mineralogy petrology* 80 (2), 189–200. doi:10.1007/BF00374895

Dong, S. W., Zhang, Y. Q., Gao, R., Su, J. B., Liu, M., and Li, J. H. (2015). A possible buried Paleoproterozoic collisional orogen beneath central South China: Evidence from seismic-reflection profiling. *Precambrian Res.* 264, 1–10. doi:10.1016/j.precamres.2015.04.003

Ducea, M. N. (2011). Fingerprinting orogenic delamination. *Geology* 39 (2), 191–192. doi:10.1130/focus022011.1

Faure, M., Chen, Y., Feng, Z. H., Shu, L. S., and Xu, Z. Q. (2017). Tectonics and geodynamics of South China: An introductory note. *J. Asian Earth Sci.* 141, 1–6. doi:10.1016/j.jseaes.2016.11.031

Feng, S. J., Zhao, K. D., Ling, H. F., Chen, P. R., Chen, W. F., Sun, T., et al. (2014). Geochronology, elemental and Nd–Hf isotopic geochemistry of Devonian A-type granites in central Jiangxi, South China: Constraints on petrogenesis and post-collisional extension of the Wuyi–Yunkai orogeny. *Lithos* 206-207, 1–18. doi:10.1016/j.lithos.2014.07.007

Feng, Z. T., Chu, Y., Wei, W., Lin, W., Xin, G. Y., Wang, Y., et al. (2022). Splitting a large pluton by cretaceous crustal extension: Evolution of the ziyuan detachment and crustal thinning of the South China block. *Tectonophysics* 838, 229481. doi:10.1016/j.tecto.2022.229481

Floyd, P. A., Leveridge, B. E., Franke, W., Shail, R., and Dörr, W. (1990). Provenance and depositional environment of Rhenohercynian synorogenic greywackes from the Giessen Nappe, Germany. *Geol. Rundsch.* 79 (3), 611–626. doi:10.1007/BF01879205

Froidevaux, C., and Ricard, Y. (1987). Tectonic evolution of high plateaus. *Tectonophysics* 134 (1), 227–238. doi:10.1016/0040-1951(87)90259-9

Frost, B. R., Barnes, C. G., Collins, W. J., Arculus, R. J., Ellis, D. J., and Frost, C. D. (2001). A geochemical classification for granitic rocks. *J. Petrology* 42 (11), 2033–2048. doi:10.1093/petrology/42.11.2033

Gan, C. S., Wang, Y. J., Zhang, Y. Z., and Qian, X. (2022). Petrogenesis of late cretaceous granites and implications for W-Sn mineralization in the Youjiang basin, south China. *Ore Geol. Rev.* 144, 104846. doi:10.1016/j.oregeorev.2022.104846

Griffin, W. L., Belousova, E. A., Shee, S. R., Pearson, N. J., and O'Reilly, S. Y. (2004). Archean crustal evolution in the northern yilgarn craton: U–Pb and Hf-isotope evidence from detrital zircons. *Precambrian Res.* 131 (3), 231–282. doi:10.1016/j.precamres.2003.12.011

Hayashi, K. I., Fujisawa, H., Holland, H. D., and Ohmoto, H. (1997). Geochemistry of ~1.9 Ga sedimentary rocks from northeastern Labrador, Canada. *Geochimica Cosmochimica Acta* 61 (19), 4115–4137. doi:10.1016/S0016-7037(97)00214-7

Healy, B., Collins, W. J., and Richards, S. W. (2004). A hybrid origin for lachlan S-type granites: The murrumbidgee batholith example. *Lithos* 78 (1), 197–216. doi:10.1016/j.lithos.2004.04.047

Hsü, K. J., Li, J. L., Chen, H. H., Wang, Q. C., Sun, S., and Şengör, A. M. C. (1990). Tectonics of south China: Key to understanding west pacific geology. *Tectonophysics* 183 (1), 9–39. doi:10.1016/0040-1951(90)90186-C

Huang, X. L., Yu, Y., Li, J., Tong, L. X., and Chen, L. L. (2013). Geochronology and petrogenesis of the early Paleozoic I-type granite in the Taishan area, South China: Middle-lower crustal melting during orogenic collapse. *Lithos* 177, 268–284. doi:10.1016/j.lithos.2013.07.002

Jia, X. H., Wang, X. D., and Yang, W. Q. (2017). Petrogenesis and geodynamic implications of the early Paleozoic potassic and ultrapotassic rocks in the South China Block. *J. Asian Earth Sci.* 135, 80–94. doi:10.1016/j.jseaes.2016.12.013

Jiang, Y. H., and Zhu, S. Q. (2017). Petrogenesis of the late jurassic peraluminous biotite granites and muscovite-bearing granites in SE China: Geochronological, elemental and Sr–Nd–O–Hf isotopic constraints. *Contributions Mineralogy Petrology* 172 (11), 101. doi:10.1007/s00410-017-1422-5

Jiao, W. F., Wu, Y. B., Yang, S. H., Peng, M., and Wang, J. (2009). The oldest basement rock in the Yangtze Craton revealed by zircon U-Pb age and Hf isotope composition. *Sci. China Ser. D Earth Sci.* 52 (9), 1393–1399. doi:10.1007/s11430-009-0135-7

Kalsbeek, F., Jepsen, H. F., and Jones, K. A. (2001). Geochemistry and petrogenesis of S-type granites in the East Greenland caledonides. *Lithos* 57 (2), 91–109. doi:10.1016/S0024-4937(01)00038-X

Kong, H., Wu, J. H., Li, H., Chen, S. F., Liu, B., and Wang, G. (2021). Early paleozoic tectonic evolution of the South China block: Constraints from geochemistry and geochronology of granitoids in hunan province. *Lithos* 380-381, 105891. doi:10.1016/j.lithos.2020.105891

Le Maitre, R. W., Streckeisen, A., Zanettin, B., Le Bas, M., Bonin, B., and Bateman, P. (2005). *Igneous rocks: A classification and glossary of terms: Recommendations of the international union of geological Sciences subcommission on the systematics of igneous rocks.* Cambridge University Press.

Li, L. M., Sun, M., Wang, Y. J., Xing, G. F., Zhao, G. C., Lin, S. F., et al. (2011). U–Pb and Hf isotopic study of zircons from migmatised amphibolites in the Cathaysia Block: Implications for the early Paleozoic peak tectonothermal event in Southeastern China. *Gondwana Res.* 19 (1), 191–201. doi:10.1016/j.gr.2010.03.009

Li, W. X., Li, X. H., and Li, Z. X. (2005). Neoproterozoic bimodal magmatism in the Cathaysia Block of South China and its tectonic significance. *Precambrian Res.* 136 (1), 51–66. doi:10.1016/j.precamres.2004.09.008

Li, X. H., Li, Z. X., Ge, W. C., Zhou, H. W., Li, W. X., Liu, Y., et al. (2003). Neoproterozoic granitoids in south China: Crustal melting above a mantle plume at ca 825 Ma? *Precambrian Res.* 122 (1), 45–83. doi:10.1016/S0301-9268(02)00207-3

Li, Z. X., and Li, X. H. (2007). formation of the 1300-km-wide intracontinental orogen and postorogenic magmatic province in mesozoic south China: A flat-slab subduction model. *Geology* 35 (2), 179–182. doi:10.1130/g23193a.1

Li, Z. X., Li, X. H., Wartho, J. A., Clark, C., Li, W. X., Zhang, C. L., et al. (2010). Magmatic and metamorphic events during the early Paleozoic Wuyi-Yunkai orogeny, southeastern South China: New age constraints and pressure-temperature conditions. *GSA Bull.* 122 (5-6), 772–793. doi:10.1130/b30021.1

Lin, S. P., Wu, J., Huang, W. T., Zhang, J., Chen, X. L., and Liang, H. Y. (2017). Zircon U-Pb ages of ore-bearing intrusions in Jiepai W (Cu) deposit northeastern Guangxi and implication on Caledonian mineralization in South China. *Geotect. Metallogenia* 41 (6), 1116–1127. (in Chinese with English Abstract). doi:10.16539/j.ddgzyckx.2017.06.009

Lin, W., Wang, Q. C., and Chen, K. (2008). Phanerozoic tectonics of south China block: New insights from the polyphase deformation in the Yunkai massif. *TECTONICS* 27 (6). doi:10.1029/2007TC002207

Liu, R., Zhou, H. W., Zhang, L., Zhong, Z. Q., Zeng, W., Xiang, H., et al. (2009). Paleoproterozoic reworking of ancient crust in the Cathaysia Block, South China: Evidence from zircon trace elements, U-Pb and Lu-Hf isotopes. *Chin. Sci. Bull.* 54 (9), 1543–1554. doi:10.1007/s11434-009-0096-4

Liu, R., Zhou, H. W., Zhang, L., Zhong, Z. Q., Zeng, W., Xiang, H., et al. (2010). Zircon U–Pb ages and Hf isotope compositions of the Mayuan migmatite complex, NW Fujian Province, Southeast China: Constraints on the timing and nature of a regional tectonothermal event associated with the Caledonian orogeny. *Lithos* 119 (3), 163–180. doi:10.1016/j.lithos.2010.06.004

Liu, S. F., Peng, S. B., Kusky, T., Polat, A., and Han, Q. S. (2018). Origin and tectonic implications of an early paleozoic (460–440 Ma) subduction-accretion shear zone in the northwestern yunkai domain, south China. *Lithos* 322, 104–128. doi:10.1016/j.lithos.2018.10.006

Liu, X. J., Zhang, Z. G., Xu, J. F., Xiao, W. J., Shi, Y., Gong, X. H., et al. (2020b). The youngest permian ocean in central asian orogenic belt: Evidence from geochronology and geochemistry of bingdaban ophiolitic mélange in central tianshan, northwestern China. *Geol. J.* 55 (3), 2062–2079. doi:10.1002/gj.3698

Liu, X., Wang, Q., Ma, L., Yang, J. H., Gou, Q., Ou, Q., et al. (2020a). Early Paleozoic intracontinental granites in the Guangzhou region of South China: Partial melting of a metasediment-dominated crustal source. *Lithos* 376-377, 105763. doi:10.1016/j.lithos.2020.105763

Loiselle, M. C., and Wones, D. R. (1979). Characteristics and origin of anorogenic granites. *Geol. Soc. Am. Abstr. programs* 11 (7), 468.

McLennan, S. M., Hemming, S., McDaniel, D. K., and Hanson, G. N. (1993). Geochemical approaches to sedimentation, provenance, and tectonics. *Geol. Soc. Am. Special Pap.* 284, 21–40. doi:10.1130/SPE284-p21

McLennan, S. M., and Taylor, S. R. (1991). Sedimentary rocks and crustal evolution: Tectonic setting and secular trends. *J. Geol.* 99 (1), 1–21. doi:10.1086/629470

Murphy, J. B., and Dostal, J. (2007). Continental mafic magmatism of different ages in the same terrane: Constraints on the evolution of an enriched mantle source. *Geology* 35 (4), 335–338. doi:10.1130/G23072A.1

Nagarajan, R., Armstrong-Altrin, J. S., Kessler, F. L., Hidalgo-Moral, E. L., Dodge-Wan, D., and Taib, N. I. (2015). Provenance and tectonic setting of Miocene siliciclastic sediments, Sibuti formation, northwestern Borneo. *Arabian J. Geosciences* 8 (10), 8549–8565. doi:10.1007/s12517-015-1833-4

Nesbitt, H. W., and Young, G. M. (1982). Early Proterozoic climates and plate motions inferred from major element chemistry of lutites. *nature* 299 (5885), 715–717. doi:10.1038/299715a0

Peng, S. B., Liu, S. F., Lin, M. S., Wu, C. F., and Han, Q. S. (2016a). Early paleozoic subduction in Cathaysia (I): New evidence from Nuodong ophiolite. *Earth Sci.* 41 (5), 765–778. (in Chinese with English abstract).

Peng, S. B., Liu, S. F., Lin, M. S., Wu, C. F., and Han, Q. S. (2016b). Early paleozoic subduction in Cathaysia (II): New evidence from the dashuang high magnesian-magnesian andesite. *Earth Sci.* 41 (6), 931–947. (in Chinese with English abstract).

Qin, X. F., Wang, Z. Q., Gong, J. H., Zhao, G. Y., Shi, H., Zhan, J. Y., et al. (2017). The confirmation of caledonian intermediate-mafic volcanic rocks in northern margin of yunkai block: Evidence for early paleozoic paleo-ocean basin in southwestern segment of qinzhou-hangzhou joint belt. *Acta Petrol. Sin.* 33 (3), 791–809. (in Chinese with English abstract).

Qin, X. F., Wang, Z. Q., Zhang, Y. L., Pan, L. Z., Hu, G. A., and Zhou, F. S. (2011). Geochronology and geochemistry of early mesozoic acid volcanic rocks from southwest Guangxi: Constraints on tectonic evolution of the southwestern segment of qinzhou-hangzhou joint belt. *Acta Petrol. Sin.* 27 (3), 794–808. (in Chinese with English Abstract).

Qiu, Y. M., Gao, S., McNaughton, N. J., Groves, D. I., and Ling, W. L. (2000). First evidence of >3.2 Ga continental crust in the Yangtze craton of south China and its implications for Archean crustal evolution and Phanerozoic tectonics. *Geology* 28 (1), 11–14. doi:10.1130/0091-7613(2000)028<0011:FEOGCC>2.0.CO;2

Reichardt, H., and Weinberg, R. F. (2012). Hornblende chemistry in meta- and diatexites and its retention in the source of leucogranites: An example from the karakoram shear zone, NW India. *J. Petrology* 53 (6), 1287–1318. doi:10.1093/petrology/egs017

Rickwood, P. C. (1989). Boundary lines within petrologic diagrams which use oxides of major and minor elements. *lithos* 22 (4), 247–263. doi:10.1016/0024-4937(89)90028-5

Roser, B. P., Coombs, D. S., Korsch, R. J., and Campbell, J. D. (2002). Whole-rock geochemical variations and evolution of the arc-derived Murihiku Terrane, New Zealand. *Geol. Mag.* 139 (6), 665–685. doi:10.1017/S0016756802006945

Rudnick, R., and Gao, S. (2003). The role of lower crustal recycling in continent formation. *Geochimica Cosmochimica Acta Suppl.* 67 (18), 403.

Sami, M., Mahdy, N. M., Ntaflos, T., and Fathy, D. (2020). Composition and origin of Ti–Nb–Ta–Zr bearing minerals in the Abu Diab highly evolved granite from the Central Eastern Desert of Egypt. *J. Afr. Earth Sci.* 165, 103808. doi:10.1016/j.jafrearsci.2020.103808

Scherer, E., Münker, C., and Mezger, K. (2001). Calibration of the lutetium-hafnium clock. *Science* 293 (5530), 683–687. doi:10.1126/science.1061372

Shu, L. S. (2012). An analysis of principal features of tectonic evolution in South China Block. *Geol. Bull. China* 31 (07), 1035–1053. (in Chinese with English Abstract). doi:10.3969/j.issn.1671-2552.2012.07.003

Shu, L. S., Faure, M., Jiang, S. Y., Yang, Q., and Wang, Y. J. (2006). SHRIMP zircon U-Pb age, litho- and biostratigraphic analyses of the Huaiyu Domain in South China — evidence for a Neoproterozoic orogen, not Late Paleozoic-Early Mesozoic collision. *Int. Union Geol. Sci.* 29 (4), 244–252. doi:10.18814/epiiugs/2006/v29i4/002

Shu, L. S., Jahn, B. M., Charvet, J., Santosh, M., Wang, B., Xu, X. S., et al. (2014). Early Paleozoic depositional environment and intraplate tectono-magmatism in the Cathaysia Block (South China): Evidence from stratigraphic, structural, geochemical and geochronological investigations. *Am. J. Sci.* 314 (1), 154. doi:10.2475/01.2014.05

Shu, L. S., Wang, B., Cawood, P. A., Santosh, M., and Xu, Z. Q. (2015). Early paleozoic and early mesozoic intraplate tectonic and magmatic events in the Cathaysia block, south China. *Tectonics* 34 (8), 1600–1621. doi:10.1002/2015TC003835

Song, Z. T., and Xu, X. S. (2022). Petrogenesis of high-maficity S-type granites: Insight from the early paleozoic jinxi granite, south China. *Lithos* 412-413, 106597. doi:10.1016/j.lithos.2022.106597

Sylvester, P. J. (1998). Post-collisional strongly peraluminous granites. *Lithos* 45 (1), 29–44. doi:10.1016/S0024-4937(98)00024-3

Tang, Y. L., Shi, Y., Hu, X. M., Liu, X. J., and Huang, C. W. (2021). Petrogenesis of early paleozoic I-type granitoids in the wuyi-yunkai orogen, south China: Implications for the tectono-magmatic evolution of the Cathaysia block. *J. Asian Earth Sci.* 220, 104906. doi:10.1016/j.jseaes.2021.104906

Taylor, S. R., and McLennan, S. M. (1985). *The continental crust: Its composition and evolution*. United Kingdom: Oxford.

Villaros, A., Buick, I. S., and Stevens, G. (2012). Isotopic variations in S-type granites: An inheritance from a heterogeneous source? *Contributions Mineralogy Petrology* 163 (2), 243–257. doi:10.1007/s00410-011-0673-9

Wang, K., Li, Z. X., Dong, S. W., Cui, J. J., Han, B. F., Zheng, T., et al. (2018). Early crustal evolution of the Yangtze Craton, South China: New constraints from zircon U-Pb-Hf isotopes and geochemistry of ca. 2.9–2.6 Ga granitic rocks in the Zhongxiang Complex. *Precambrian Res.* 314, 325–352. doi:10.1016/j.precamres.2018.05.016

Wang, X. L., Zhao, G. C., Zhou, J. C., Liu, Y. S., and Hu, J. (2008). Geochronology and Hf isotopes of zircon from volcanic rocks of the Shuangqiaoshan Group, South China: Implications for the Neoproterozoic tectonic evolution of the eastern Jiangnan orogen. *Gondwana Res.* 14 (3), 355–367. doi:10.1016/j.gr.2008.03.001

Wang, X. L., Zhou, J. C., Griffin, W. L., Wang, R. C., Qiu, J. S., O'Reilly, S. Y., et al. (2007a). Detrital zircon geochronology of precambrian basement sequences in the jiangnan orogen: Dating the assembly of the Yangtze and Cathaysia blocks. *Precambrian Res.* 159 (1), 117–131. doi:10.1016/j.precamres.2007.06.005

Wang, Y. J., Fan, W. M., Zhang, G. W., and Zhang, Y. H. (2013a). Phanerozoic tectonics of the South China block: Key observations and controversies. *Gondwana Res.* 23 (4), 1273–1305. doi:10.1016/j.gr.2012.02.019

Wang, Y. J., Fan, W. M., Zhao, G. C., Ji, S. C., and Peng, T. P. (2007b). Zircon U–Pb geochronology of gneissic rocks in the Yunkai massif and its implications on the Caledonian event in the South China Block. *Gondwana Res.* 12 (4), 404–416. doi:10.1016/j.gr.2006.10.003

Wang, Y. J., Zhang, A. M., Fan, W. M., Zhang, Y. H., and Zhang, Y. Z. (2013b). Origin of paleosubduction-modified mantle for Silurian gabbro in the Cathaysia Block: Geochronological and geochemical evidence. *Lithos* 160-161, 37–54. doi:10.1016/j.lithos.2012.11.004

Wang, Y. J., Zhang, A. M., Fan, W. M., Zhao, G. C., Zhang, G. W., Zhang, Y. Z., et al. (2011). Kwangsian crustal anatexis within the eastern South China Block: Geochemical, zircon U–Pb geochronological and Hf isotopic fingerprints from the gneissoid granites of Wugong and Wuyi–Yunkai Domains. *Lithos* 127 (1), 239–260. doi:10.1016/j.lithos.2011.07.027

Wang, Y. J., Zhang, F. F., Fan, W. M., Zhang, G. W., Chen, S. Y., Cawood, P. A., et al. (2010). Tectonic setting of the South China Block in the early Paleozoic: Resolving intracontinental and ocean closure models from detrital zircon U-Pb geochronology. *Tectonics* 29 (6), TC6020. doi:10.1029/2010TC002750

Wang, Y. N., Li, G. J., Wang, Q. F., Santosh, M., and Chen, J. H. (2020). Early paleozoic granitoids from south China: Implications for understanding the wuyi-yunkai orogen. *Int. Geol. Rev.* 62 (2), 243–261. doi:10.1080/00206814.2019.1600437

Whalen, J. B., Currie, K. L., and Chappell, B. W. (1987). A-Type granites: Geochemical characteristics, discrimination and petrogenesis. *Contributions mineralogy petrology* 95 (4), 407–419. doi:10.1007/BF00402202

Wronkiewicz, D. J., and Condie, K. C. (1987). Geochemistry of archean shales from the witwatersrand supergroup, south Africa: Source-area weathering and provenance. *Geochimica Cosmochimica Acta* 51 (9), 2401–2416. doi:10.1016/0016-7037(87)90293-6

Wu, F. Y., Li, X. H., Zheng, Y. F., and Gao, S. (2007). Lu-Hf isotopic systematics and their applications in petrology. *Acta. petr. Sin.* 23 (2), 185–220. doi:10.3969/j.issn.1000-0569.2007.02.001

Wu, J., Liang, H. Y., Huang, W. T., Wang, C. L., Sun, W. D., Sun, Y. L., et al. (2012). Indosinian isotope ages of plutons and deposits in southwestern Miaoershan-Yuechengling, northeastern Guangxi and implications on Indosinian mineralization in South China. *Chin. Sci. Bull.* 57 (9), 1024–1035. doi:10.1007/s11434-011-4968-z

Xia, Y., Xu, X. S., Zou, H. B., and Liu, L. (2014). Early paleozoic crust–mantle interaction and lithosphere delamination in south China block: Evidence from geochronology, geochemistry, and Sr–Nd–Hf isotopes of granites. *Lithos* 184-187, 416–435. doi:10.1016/j.lithos.2013.11.014

Xiang, Z. J., Yan, Q. R., White, J. D. L., Song, B., and Wang, Z. Q. (2015). Geochemical constraints on the provenance and depositional setting of Neoproterozoic volcaniclastic rocks on the northern margin of the Yangtze Block, China: Implications for the tectonic evolution of the northern margin of the Yangtze Block. *Precambrian Res.* 264, 140–155. doi:10.1016/j.precamres.2015.04.012

Xin, Y. J., Li, J. H., Ratschbacher, L., Zhao, G. C., Zhang, Y. Q., Dong, S. W., et al. (2020). Early devonian (415–400 Ma) A-type granitoids and diabases in the wuyishan, eastern Cathaysia: A signal of crustal extension coeval with the separation of south China from gondwana. *GSA Bull.* 132 (11-12), 2295–2317. doi:10.1130/B35412.1

Xu, W. J., and Xu, X. S. (2015). Early paleozoic intracontinental felsic magmatism in the South China block: Petrogenesis and geodynamics. *Lithos* 234-235, 79–92. doi:10.1016/j.lithos.2015.08.006

Yan, Z., Wang, Z., Yan, Q., Wang, T., and Guo, X. (2012). Geochemical constraints on the provenance and depositional setting of the devonian liuling group, East qinling mountains, central China: Implications for the tectonic evolution of the qinling orogenic belt. *J. Sediment. Res.* 82 (1), 9–20. doi:10.2110/jsr.2012.4

Yang, F., Feng, Z. H., Kang, Z. Q., and Xiao, R. (2011). Muscovite 40Ar-39Ar age of the Damingshan tungsten deposit in central Guangxi and its geological significance. *Geol. Bull. China* 30 (09), 1429–1433. (in Chinese with English Abstract).

Yao, J. L., Shu, L. S., Santosh, M., and Zhao, G. C. (2014). Neoproterozoic arc-Related mafic–ultramafic rocks and syn-collision granite from the Western segment of the jiangnan orogen, south China: Constraints on the neoproterozoic assembly of the Yangtze and Cathaysia blocks. *Precambrian Res.* 243, 39–62. doi:10.1016/j.precamres.2013.12.027

Yao, W. H., Li, Z. X., Li, W. X., Wang, X. C., Li, X. H., and Yang, J. H. (2012). Post-kinematic lithospheric delamination of the Wuyi–Yunkai orogen in South China: Evidence from ca 435Ma high-Mg basalts. *Lithos* 154, 115–129. doi:10.1016/j.lithos.2012.06.033

Yu, J. H., O'Reilly, S. Y., Wang, L. J., Griffin, W. L., Zhou, M. F., Zhang, M., et al. (2010). Components and episodic growth of Precambrian crust in the Cathaysia Block, South China: Evidence from U–Pb ages and Hf isotopes of zircons in Neoproterozoic sediments. *Precambrian Res.* 181 (1), 97–114. doi:10.1016/j.precamres.2010.05.016

Yu, J. H., Wang, L. J., O'Reilly, S. Y., Griffin, W. L., Zhang, M., Li, C. Z., et al. (2009). A Paleoproterozoic orogeny recorded in a long-lived cratonic remnant (Wuyishan terrane), eastern Cathaysia Block, China. *Precambrian Res.* 174 (3), 347–363. doi:10.1016/j.precamres.2009.08.009

Yu, J. H., Wang, L. J., Wei, Z. Y., Sun, T., and Shu, L. S. (2007). Phanerozoic metamorphic episodes and characteristics of Cathaysia block. *Geol. J. China Univ.* 13 (3), 474–483. (in Chinese with English abstract). doi:10.3969/j.issn.1006-7493.2007.03.016

Yu, J. H., Xu, X. S., O'Reilly, S. Y., Griffin, W. L., and Zhang, M. (2003). Granulite xenoliths from Cenozoic Basalts in SE China provide geochemical fingerprints to distinguish lower crust terranes from the North and South China tectonic blocks. *Lithos* 67 (1), 77–102. doi:10.1016/S0024-4937(02)00253-0

Yu, W. C., Du, Y. S., Cawood, P. A., Xu, Y. J., and Yang, J. H. (2015). Detrital zircon evidence for the reactivation of an Early Paleozoic syn-orogenic basin along the North Gondwana margin in South China. *Gondwana Res.* 28 (2), 769–780. doi:10.1016/j.gr.2014.07.014

Yu, Y., Huang, X. L., He, P. L., and Li, J. (2016). I-type granitoids associated with the early Paleozoic intracontinental orogenic collapse along pre-existing block boundary in South China. *Lithos* 248-251, 353–365. doi:10.1016/j.lithos.2016.02.002

Zen, E. (1986). Aluminum enrichment in silicate melts by fractional crystallization: Some mineralogic and petrographic constraints. *J. Petrology* 27 (5), 1095–1117. doi:10.1093/petrology/27.5.1095

Zhang, F. F., Wang, Y. J., Zhang, A. M., Fan, W. M., Zhang, Y. Z., and Zi, J. W. (2012). Geochronological and geochemical constraints on the petrogenesis of Middle Paleozoic (Kwangsian) massive granites in the eastern South China Block. *Lithos* 150, 188–208. doi:10.1016/j.lithos.2012.03.011

Zhang, G. W., Guo, A. L., Wang, Y. J., Li, S. Z., Dong, Y. P., Liu, S. F., et al. (2013). Tectonics of South China continent and its implications. *Sci. China(Earth Sci.* 56 (11), 1804–1828. doi:10.1007/s11430-013-4679-1

Zhang, Q., Jiang, Y. H., Wang, G. C., Liu, Z., Ni, C. Y., and Qing, L. (2015). Origin of Silurian gabbros and I-type granites in central Fujian, SE China: Implications for the evolution of the early Paleozoic orogen of South China. *Lithos* 216-217, 285–297. doi:10.1016/j.lithos.2015.01.002

Zhang, W. L., Che, X. D., Chen, W. D., Wang, R. C., and Zhang, D. (2017a). A new potential caledonian–indosinian ore concentration area: Evidence from diagenesis and mineralization ages of the miao'ershan–yuechengling region. *Acta Geol. Sin. - Engl. Ed.* 91 (2), 743–744. doi:10.1111/1755-6724.13136

Zhang, X. S., Xu, X. S., Xia, Y., and Liu, L. (2017b). Early Paleozoic intracontinental orogeny and post-orogenic extension in the South China Block: Insights from volcanic rocks. *J. Asian Earth Sci.* 141, 24–42. doi:10.1016/j.jseaes.2016.07.016

Zhao, G. C. (2015). Jiangnan orogen in south China: Developing from divergent double subduction. *Gondwana Res.* 27 (3), 1173–1180. doi:10.1016/j.gr.2014.09.004

Zhao, J. H., Yang, T., and Wang, W. (2022). Orogenic belt resulting from ocean-continent collision. *GEOLOGY* 50 (11), 1266–1269. doi:10.1130/G50337.1

Zhao, K. D., Jiang, S. Y., Sun, T., Chen, W. F., Ling, H. F., and Chen, P. R. (2013). Zircon U-Pb dating, trace element and Sr-Nd-Hf isotope geochemistry of Paleozoic granites in the Miao'ershan-Yuechengling batholith, South China: Implication for petrogenesis and tectonic-magmatic evolution. *J. Asian Earth Sci.* 74, 244–264. doi:10.1016/j.jseaes.2012.12.026

Zhao, P. L., Yuan, S. D., Mao, J. W., Santosh, M., Li, C., and Hou, K. J. (2016). Geochronological and petrogeochemical constraints on the skarn deposits in Tongshanling ore district, southern Hunan Province: Implications for Jurassic Cu and W metallogenic events in South China. *Ore Geol. Rev.* 78, 120–137. doi:10.1016/j.oregeorev.2016.03.004

Zhong, Y. F., Ma, C. Q., Liu, L., Zhao, J. H., Zheng, J. P., Nong, J. N., et al. (2014). Ordovician appinites in the Wugongshan Domain of the Cathaysia Block, South China: Geochronological and geochemical evidence for intrusion into a local extensional zone

within an intracontinental regime. *Lithos* 198-199, 202–216. doi:10.1016/j.lithos.2014.04.002

Zhong, Y. F., Ma, C. Q., Zhang, C., Wang, S. M., She, Z. B., Liu, L., et al. (2013). Zircon U–Pb age, Hf isotopic compositions and geochemistry of the Silurian Fengdingshan I-type granite Pluton and Taoyuan mafic–felsic Complex at the southeastern margin of the Yangtze Block. *J. Asian Earth Sci.* 74, 11–24. doi:10.1016/j.jseaes.2013.05.025

Zhong, Y. F., Wang, L. X., Zhao, J. H., Liu, L., Ma, C. Q., Zheng, J. P., et al. (2016). Partial melting of an ancient sub-continental lithospheric mantle in the early Paleozoic intracontinental regime and its contribution to petrogenesis of the coeval peraluminous granites in South China. *Lithos* 264, 224–238. doi:10.1016/j.lithos.2016.08.026

Zhou, J. F. (2020). *Geochemical characteristics and genesis of zhenxu talc deposit in the southeastern of Youjiang fold belt*. East China University Of Technology. Master.

Zhou, Z. B., and Wen, H. J. (2021). A magmatic-hydrothermal indium-bearing polymetallic vein mineralization belt in the Western Jiangnan Orogen: Evidence from zinc and cadmium isotopes of sphalerite. *Ore Geol. Rev.* 131, 103843. doi:10.1016/j.oregeorev.2020.103843

Zhu, Y., Lai, S. C., Qin, J. F., Zhu, R. Z., Zhang, F. Y., and Zhang, Z. Z. (2020). Petrogenesis and geochemical diversity of late mesoproterozoic S-type granites in the Western Yangtze block, south China: Co-Entrainment of peritectic selective phases and accessory minerals. *Lithos* 352-353, 105326. doi:10.1016/j.lithos.2019.105326